ELSEVIER

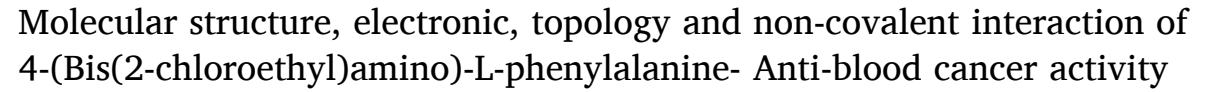
Contents lists available at ScienceDirect

# **Chemical Physics Impact**

journal homepage: www.sciencedirect.com/journal/chemical-physics-impact



# Full Length Article



K. Parveen Begaum <sup>a,\*</sup>, T. Prabhu <sup>a,\*</sup>, M. Thirunavukkarasu <sup>b</sup>, P. Sangeetha <sup>c</sup>, Saleem Javed <sup>d</sup>, Jamal M. Khaled <sup>e</sup>, Ghulam Abbas <sup>f</sup>, S. Muthu <sup>g,\*</sup>

- a Department of Physics, A.V.C.College (Autonomous), Myladuthurai 609305, Affiliated to Bharathidasan University, Tiruchirappali-24, Tamilnadu, India
- b Department of Physics, School of Science and Humanities, Vel Tech Rangarajan Dr. Sagunthala R&D Institute of Science and Technology, Avadi, Chennai 600062, India
- <sup>c</sup> Department of Physics, Panimalar Engineering College, Chennai 600 123, Tamilnadu, India
- <sup>d</sup> Department of Chemistry, Jamia Millia Islamia, New Delhi 110025, India
- e Department of Botany and Microbiology, College of Science, King Saud University, P. O. Box 2455, Riyadh 11451, Saudi Arabia
- f Institute of Inorganic Chemistry, Karlsruhe Institute of Technology, Engesserstr 15, 76131 Karlsruhe, Germany
- g Department of Physics, Arignar Anna Govt. Arts College, Cheyyar 604407, Tamil Nadu, India

#### ARTICLE INFO

# Keywords: Density functional theory Natural bond orbital analysis, Atoms in molecule (AIM), Reduced density gradient (RDG) Molecular docking

#### ABSTRACT

In this study, it is attempted to scrutinize the global minimum energy structure of anti-blood cancer drug 4-(Bis (2-chloroethyl)amino)-L-phenylalanine (4B2CA-LPA) and functionalized density functional theory (DFT) calculations regarding their geometries, topological features of covalent, non-covalent interactions with employing Atoms in molecule (AIM) and Reduced density gradient (RDG) studies. As per the topological results, a new type of non-covalent attraction forces of hydrogen-hydrogen interaction was found in this molecule. Electrostatic potential variation as well as global reactive descriptor energy variations in the solvation phases was carried out by molecular electrostatic potential (MEP) and frontier molecular orbitals (FMOs) analysis. Moreover, the electronic excitations in liquids of 4B2CA-LPA were evaluated in UV-Vis absorptions. The local bonding electron transitions and optical properties of the compound were examined with natural bond orbital (NBO) studies. The 4B2CA-LPA molecule can serve as lead molecules for the growth of anti-blood cancer drugs. Molecular docking investigation has also been carried out to determine the ability of target molecules to bind with Hematopoietic inhibitors in blood cells.

#### 1. Introduction

Blood cancer is a malignant class of cancer disease that can develop in complete organs of the body because of the unregulated proliferation of abnormal cells. The introduction of novel medication classes [1–4], such as novel treatments for multiple myeloma (blood cell cancer), including proteasome blockers, immunoregulatory drugs, and monoclonal antibodies, have significantly changed exactly how the disease is treated, over the past 20 years [3,5-8]. The levels and degree of responsiveness, as a result, increased by including these medications in treatment regimens for patients with newly diagnosed multiple myeloma [8,9]. Further research is necessary to determine the advantages of consolidating treatment based on innovative medications following the intensifying stage [10,11], as not all studies have

supported the use of consolidation treatment after transplantation [12]. The 4-(Bis(2-chloroethyl) amino)-L-phenylalanine (4B2CA-LPA) and also known as Alkeran is anti-blood cancer (multiple myeloma) drug and it was approved melphalan by USA Food and Drug Administration five decades ago [13–16]. It functions by preventing the growth of cancer cells, which are then subsequently eliminated by the body. Melphalan may also influence the proliferation of healthy cells, therefore other negative consequences will also manifest [17–20]. Several works have already reported how the 4B2CA-LPA chemical was synthesized using many different approaches [21–23]. According to the literature, the common process for producing the title chemical, when 4-Nitro-L-phenylalanine was heated with phthalic anhydride, it was converted to phthalimide, which was subsequently modified into its ethyl ester. Catalytic hydrogenation was used to produce similar aniline. The

E-mail addresses: ttsprabhu@gmail.com (T. Prabhu), mutgee@gmail.com (S. Muthu).

https://doi.org/10.1016/j.chphi.2023.100272

<sup>\*</sup> Corresponding authors.

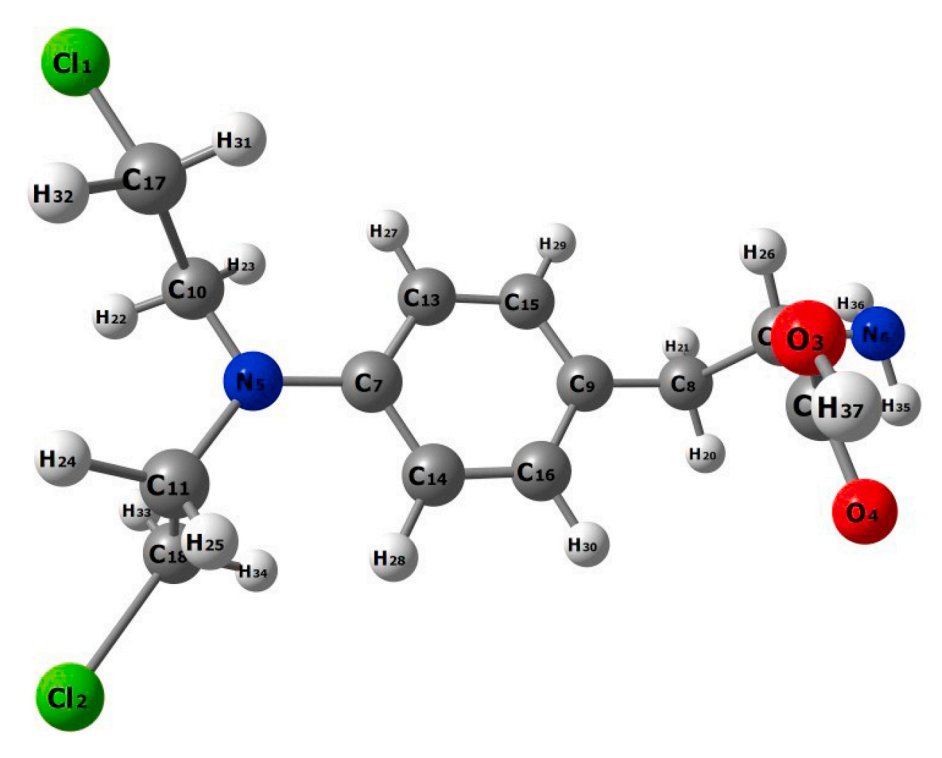


Fig. 1. Optimized stable Structure 4B2CA-LPA in the gas phase.

Table 1
Optimized parameters of the title compound: bond lengths (Å) bond angles ().

| Parameter | Bond Len | gth (Å) | Parameter   | Bond Ang | gle (°) |
|-----------|----------|---------|-------------|----------|---------|
|           | DFT      | Lit.a   |             | DFT      | Lit. a  |
| Cl1-C17   | 1.817    | 1.787   | Cl1-C17-C10 | 110.4    | 110.8   |
| Cl2-C18   | 1.817    | 1.807   | O3-C19-O4   | 123      | 126.2   |
| O3-C19    | 1.348    | 1.266   | O3-C19-C12  | 113      | 112.2   |
| O3-H37    | 0.97     | 1.006   | O4-C19-C12  | 124      | 121.6   |
| O4-C19    | 1.207    | 1.228   | C7-N5-C10   | 121.5    | 121.33  |
| N5-C7     | 1.399    | 1.471   | C7-N5-C11   | 121.5    | 122.58  |
| N5-C10    | 1.455    | 1.451   | N5-C7-C13   | 121.5    | 121.12  |
| N5-C11    | 1.455    | 1.474   | C10-N5-C11  | 116.9    | 116.4   |
| N6-C12    | 1.463    | 1.485   | N5-C10-C17  | 111.8    | 110.8   |
| N6-H35    | 1.016    | 1.063   | N5-C11-C18  | 111.8    | 110.9   |
| N6-H36    | 1.015    | 1.029   | N6-C12-C8   | 114.5    | -       |
| C7-C13    | 1.41     | 1.391   | N6-C12-C19  | 106.6    | -       |
| C7-C14    | 1.409    | 1.372   | C13-C7-C14  | 116.9    | 115.97  |
| C8-C9     | 1.511    | 1.442   | C7-C13-C15  | 121      | 121.91  |
| C8-C12    | 1.557    | 1.499   | C7-C13-H27  | 120.8    | 119.0   |
| C9-C15    | 1.398    | 1.398   | C9-C8-C12   | 115      | 115.97  |
| C9-C16    | 1.397    | 1.360   | C9-C8-H20   | 110.3    | 119.0   |
| C10-C17   | 1.531    | 1.495   | C8-C9-C15   | 121.5    | -       |
| C11-C18   | 1.531    | 1.504   | C8-C12-C19  | 109.8    | -       |
| C12-C19   | 1.523    | -       | C15-C9-C16  | 116.9    | 118.78  |
| C13-C15   | 1.39     | 1.391   | C9-C15-C13  | 122.1    | 125.06  |
| C14-C16   | 1.391    | 1.372   | C9-C16-C14  | 122      | 124.63  |

<sup>&</sup>lt;sup>a</sup> Literature values are taken from Ref. [33,34]

bischloride was created by heating oxirane in acid and then treating it with phosphorus oxychloride, finally 4-(Bis(2-chloroethyl)amino)--L-phenylalanine (Melphalan) was produced by removing the protecting groups in hydrochloric acid.

Melphalan (Alkeran) is a medication that can be used to treat multiple myeloma. To prepare patients for stem cell transplantation, it serves as a conditioning therapy. For individuals who are unable to take melphalan orally, there is also an available liquid form of melphalan (melphalan hydrochloride). Hence the researchers need more about the physicochemical properties of 4B2CA-LPA and the influence of molecule in liquid phases (solvent effects), Melphalan is used in advanced therapy

for the treatment of developing medication carriers for multiple myeloma that minimize the toxicity, the chemical and biological modifications of the 4B2CA-LPA molecule to increase anticancer activity and integrating therapies to improve the efficiency of cancer treatment. Due to fact that the use of 4B2CA-LPA in the treatment of different tumor cell types is currently being researched and a large number of research articles have been published. To the best of my knowledge, no DFT investigations using topological analysis, solvation effects, reactivitybased descriptor analyses and vibrational studies have ever been conducted on this drug. In recent years, the study of theoretical modeling of cancer drug molecules with medical significance has benefited from the development of computer simulators, and it is now able to assess the important physical and chemical properties of approved drug compounds for cancer treatment using a range of theoretical methodologies [24]. Density functional theory (DFT) has advanced with the establishment of a much more accurate exchange-correlation function and has developed into a magnificent tool in comparison to other traditional approaches because of its low processing cost and excellent accuracy [25].

In the present investigation, the focus of our study has been on figuring out how to drug material's molecular geometry by connecting the desired attributes from an experimental assessment with the expected theoretical parameters of DFT. The physicochemical properties of vibrational assessment with IR and Raman spectra, topological analysis (RDG, LOL, ELF & AIM), solvation effects on reactivity descriptors (MEP & FMOs), natural bond orbital studies, and electronic structure assessments (UV-Vis, MEP & FMOs) in various liquids are all being investigated using the DFT methods. Finally, molecular docking was carried out using three different blood cancer proteins (PDB codes: 4FVR, 3WIX, & 5UUT) based on the PASS Online tool's prediction with the highest probability activity (Pa). We chose them for the current studies based on the literature review since the title chemical 4B2CA-LPA has not been previously investigated with these specific blood cell proteins.

### 2. Quantum computational details

The compound's complete molecular geometry optimization was

**Table 2**Topological parameters of the **4B2CA-LPA** for covalent and non-covalent interactions in gas phases.

| BCP       | ρ(r) (a.u) | $ abla^2 \rho(\mathbf{r}) \text{ (a.u)}$ | V(r) (a.u) | G (r) (a.u) | H(r) (a.u) | -(G/V) | ε      |
|-----------|------------|--|------------|-------------|------------|--------|--------|
| C10 - C17 | 0.2454     | -0.5626                                  | -0.2516    | 0.0555      | -0.1961    | 0.2204 | 0.0650 |
| C10 - H22 | 0.2813     | -0.9582                                  | -0.3170    | 0.0387      | -0.2783    | 0.1221 | 0.0276 |
| C10 - H23 | 0.2825     | -0.9647                                  | -0.3173    | 0.0381      | -0.2792    | 0.1199 | 0.0268 |
| C11 - C18 | 0.2454     | -0.5627                                  | -0.2516    | 0.0554      | -0.1961    | 0.2204 | 0.0651 |
| C11 - H24 | 0.2813     | -0.9578                                  | -0.3168    | 0.0387      | -0.2781    | 0.1221 | 0.0276 |
| C11 - H25 | 0.2825     | -0.9649                                  | -0.3172    | 0.0380      | -0.2792    | 0.1198 | 0.0267 |
| C12 - C19 | 0.2554     | -0.6309                                  | -0.2713    | 0.0568      | -0.2145    | 0.2092 | 0.0387 |
| C12 - H26 | 0.2841     | -0.9767                                  | -0.3194    | 0.0376      | -0.2818    | 0.1178 | 0.0192 |
| C13 - C15 | 0.3092     | -0.8574                                  | -0.4193    | 0.1025      | -0.3168    | 0.2444 | 0.2239 |
| C13 - H27 | 0.2818     | -0.9607                                  | -0.3244    | 0.0421      | -0.2823    | 0.1298 | 0.0291 |
| C14 - C16 | 0.3087     | -0.8547                                  | -0.4174    | 0.1019      | -0.3155    | 0.2440 | 0.2203 |
| C14 - H28 | 0.2818     | -0.9607                                  | -0.3244    | 0.0421      | -0.2823    | 0.1298 | 0.0292 |
| C15 - H29 | 0.2801     | -0.9572                                  | -0.3178    | 0.0392      | -0.2785    | 0.1235 | 0.0173 |
| C16 - H30 | 0.2813     | -0.9659                                  | -0.3181    | 0.0383      | -0.2798    | 0.1204 | 0.0172 |
| C17 - H31 | 0.2854     | -0.9874                                  | -0.3199    | 0.0365      | -0.2834    | 0.1142 | 0.0237 |
| C17 - H32 | 0.2841     | -0.9787                                  | -0.3188    | 0.0371      | -0.2817    | 0.1163 | 0.0243 |
| C18 - H33 | 0.2841     | -0.9785                                  | -0.3188    | 0.0371      | -0.2817    | 0.1163 | 0.0243 |
| C18 - H34 | 0.2854     | -0.9872                                  | -0.3199    | 0.0365      | -0.2833    | 0.1142 | 0.0237 |
| C7 - C13  | 0.2997     | -0.8095                                  | -0.3931    | 0.0954      | -0.2977    | 0.2426 | 0.2172 |
| C7 - C14  | 0.3001     | -0.8114                                  | -0.3946    | 0.0959      | -0.2987    | 0.2430 | 0.2189 |
| C8 - C12  | 0.2306     | -0.4840                                  | -0.2288    | 0.0539      | -0.1749    | 0.2356 | 0.0368 |
| C8 - C9   | 0.2496     | -0.5833                                  | -0.2625    | 0.0584      | -0.2042    | 0.2223 | 0.0422 |
| C8 - H20  | 0.2762     | -0.9210                                  | -0.3133    | 0.0415      | -0.2718    | 0.1325 | 0.0070 |
| C8 - H21  | 0.2739     | -0.9064                                  | -0.3126    | 0.0430      | -0.2696    | 0.1376 | 0.0078 |
| C9 - C15  | 0.3070     | -0.8467                                  | -0.4111    | 0.0997      | -0.3114    | 0.2425 | 0.2102 |
| C9 - C16  | 0.3071     | -0.8467                                  | -0.4116    | 0.1000      | -0.3117    | 0.2429 | 0.2125 |
| Cl1 - C17 | 0.1686     | -0.1849                                  | -0.1591    | 0.0564      | -0.1027    | 0.3547 | 0.0067 |
| Cl2 - C18 | 0.1687     | -0.1852                                  | -0.1592    | 0.0564      | -0.1027    | 0.3546 | 0.0066 |
| H23 - H27 | 0.0139     | 0.0544                                   | -0.0087    | 0.0111      | 0.0025     | 1.2825 | 0.7384 |
| H25 - H28 | 0.0139     | 0.0543                                   | -0.0087    | 0.0111      | 0.0025     | 1.2828 | 0.7486 |
| N5 - C10  | 0.2623     | -0.6827                                  | -0.4175    | 0.1234      | -0.2941    | 0.2956 | 0.0482 |
| N5 - C11  | 0.2622     | -0.6823                                  | -0.4174    | 0.1234      | -0.2940    | 0.2957 | 0.0482 |
| N5 - C7   | 0.2916     | -0.8053                                  | -0.5407    | 0.1697      | -0.3710    | 0.3138 | 0.1153 |
| N6 - C12  | 0.2656     | -0.6845                                  | -0.3783    | 0.1036      | -0.2747    | 0.2739 | 0.0532 |
| N6 - H35  | 0.3362     | -1.5132                                  | -0.4963    | 0.0590      | -0.4373    | 0.1189 | 0.0492 |
| N6 - H36  | 0.3368     | -1.4872                                  | -0.4934    | 0.0608      | -0.4326    | 0.1232 | 0.0499 |
| O3 - C19  | 0.3001     | -0.4745                                  | -0.7506    | 0.3160      | -0.4346    | 0.4210 | 0.0324 |
| O3 - H37  | 0.3581     | -2.4988                                  | -0.7577    | 0.0665      | -0.6912    | 0.0878 | 0.0167 |
| O4 - C19  | 0.4173     | -0.1744                                  | -1.3767    | 0.6666      | -0.7102    | 0.4842 | 0.0737 |
| RCP a     | ρ(r) (a.u) | $\nabla^2 \rho(\mathbf{r})$ (a.u)        | V(r) (a.u) | G (r) (a.u) | H(r) (a.u) | -(G/V) | ε      |
| R1        | 0.0215     | 0.1560                                   | -0.0243    | 0.0316      | 0.007      | 1.300  | -      |
| R2        | 0.0135     | 0.0666                                   | -0.01040   | 0.0135      | 0.003      | 1.298  | -      |
| R3        | 0.0134     | 0.0664                                   | -0.01037   | 0.01349     | 0.003      | 1.301  | -      |

<sup>&</sup>lt;sup>a</sup> [R1- RCP1 (C7 C13 C15 C9 C16 C14); R2 – RCP2 (N5 C7 C13 H27 H23 C10); R3- RCP3 (N5 C7 C14 H28 H25 C11)]

done using the Gaussian 09W desktop programme and DFT at the B3LYP /6-311++G(d,p) level basis set [26]. The vibrational frequencies of the optimized molecule were evaluated at the same theoretical level, and the scaled wavenumbers were obtained by applying the standard scaling factor of 0.96 [27]. PED prediction was performed using the VEDA programme [28]. TD-DFT methodology in the gas phase, ethanol, chloroform, DMSO, methanol, and water was used to detect the electronic excitations of the title chemical. Moreover, the Multiwfn 3.6 tool was used to analyze the solvent effect on the ESP surface map as well as the topological properties of the ELF, LOL, RDG, and AIM studies [29]. Before Molecular docking, the title molecule's lower energy structure was designed then it was saved as a single document in PDB format using the PyMol programme [30]. The selected protein (PDB code: 4FVR, 3WIX & 5UUT) was then downloaded in PDB format from the online tool, then docking was performed by Autodock tools 1.5.6 [31].

# 3. Results and discussion

# 3.1. Molecular geometry

The compound **4B2CA-LPA** has the C1 point group and the chemical formula is  $C_{13}H_{18}C_{l2}N_2O_2$ . In this present work, the optimized structure of the compound was obtained by DFT at the B3LYP level and the 6-

311++G(d,p) basis set [32]. This ideal structure was found by the lowest global minimum energy of -1686.85890 Hartree (-2.6882 kcal/mol) with dipole moment 1.5384557 Debye and it was shown in Fig. 1. For the comparison of theoretical values of bond length and bond angles as the structure of the compound 4B2CA-LPA was not studied through XRD crystal investigations, hence we selected two structurally similar compound's parameters, which are listed in Table 1 [33,34]. As per the optimized result, the longest bond distance 1.817 Å, was calculated for Cl1-C17 & Cl2-C18 because the heavier chlorine molecule was attached at positions Cl1 and Cl2 and since these bonds are considered to be the weakest site in this molecule, which are good agreement with literature values (1.787 & 1.807 Å). Usually, the Cl-C bond range is 1.77-1.78 Å however, it is significantly longer and the calculated adjacent C-C bonds (C10-C17 & C11-C18) are consequently shorter (1.531 Å) because of the electronegativity difference between the atoms. Similar to this, the strongest calculated bonds in the molecule were found at O3 and C19, which had a dual attachment between them, hence the shortest distance for O3-H37 & O4-C19 are 0.97 & 1.207 Å respectively, which is also consistent with the values of literature (1.006 & 1.228 Å). This carbonyl and hydroxyl (C=O, CO & OH) groups with one aromatic ring combine to form an L-phenylalanine group in the title chemical 4B2CA-LPA. Moreover, the important calculated nitrogen attached bonds are N5-C7, N5-C10, N5-C11, N6-C12, N6-H35, and

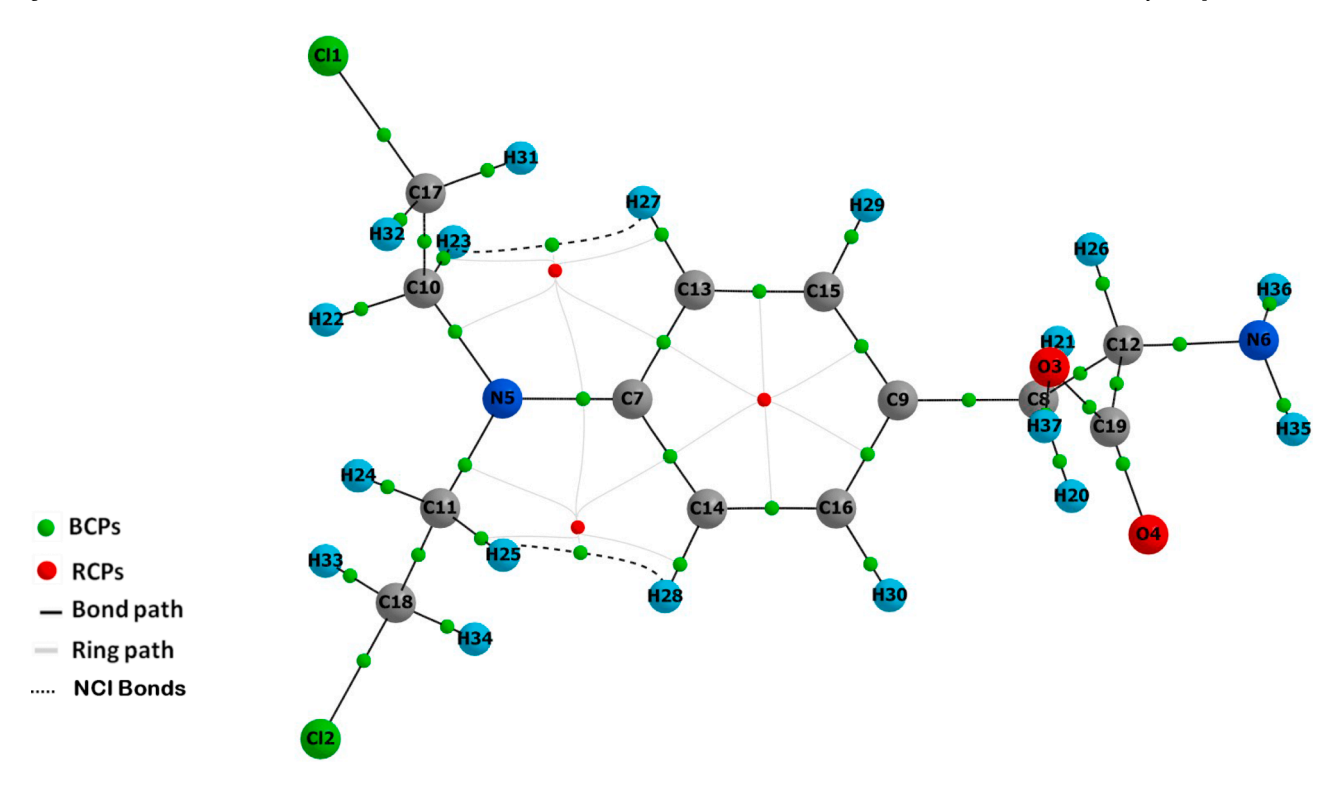


Fig. 2. AIM Molecular graph of 4B2CA-LPA: green tiny spheres (BCPs), small red spheres (RCBs), black lines (bond paths), ash color solid lines (RCP to BCP ring path), and black dotted lines (non-covalent interactions (NCI)) are illustrated in this figure.

N6-H36 with distances 1.399, 1.455, 1.455, 1.463 1.016 and 1.015 Å respectively, while the CC bonds in the benzene ring are C9-C15, C9-C16, C13-C15, C14-C16, C7-C13 C7-C14 of 1.398, 1.397 1.39, 1.391 1.41 and 1.409 Å respectively.

The 2-chloroethyl chains from N5 are stretched and separate from one another between the N5-C10 and N5-C11 bonds, with the distance found between Cl1 and Cl2 being 6.699 Å and the angle of C11-N5-C10 being  $116.9^{\circ}$ . Most of the bond angle values are very close to those that are frequently seen in structures with similar compound structures, therefore extensive discussion is not required.

# 3.2. Topological analysis

# 3.2.1. AIM analysis

Table 2 shows the 4B2CA-LPA parameters for all BCPs in the compounds under study. Fig. 2 exhibits the atomic diagram of 4B2CA-LPA as illustrated in this figure ring critical points RCP's (in a small sphere in red color), bond routes (in black color solid lines for covalent; and black color dotted lines for non-covalent paths), bond critical points BCP's (in green color small spheres with  $\nabla^2 \rho(r)$  values mentioned) [35,36]. As a result, BCPs H23...H27 and H25...H28 are subsequently formed as intramolecular hydrogen bonds in the molecular surface during optimization, and they can be identified by their positive  $\nabla^2 \rho(r)$  values (0.0544 & 0.0543 a.u.) and lowest  $\rho(r)$  vales (0.0139 & 0.0139 a.u.). Other BCPs are identified as covalent bonds by the range of  $\rho(r)$  (0.1686 to 0.4173 a.u.) and all negative (-2.4988 to -0.1744) values of  $\nabla^2 \rho(r)$ . Moreover, this AIM result shows that O4=C19 ( $\rho(r)$ = 0.4173 a.u.) has the highest computed electron density while H2-H27 and H25-H28 ( $\varepsilon=$ 0.7486 & 0.7384 a.u.) had the highest degree of electron distribution asymmetry. This may be because of the non-covalent (intramolecular hydrogen) bonds that were formed at these BCPs. In this case, three RCPs (ring critical points) were also found at R1(C7 C13 C15 C9 C16 C14), R2 (N5 C7 C13 H27 H23 C10) and R3 (N5 C7 C14 H28 H25 C11) with positive  $\nabla^2 \rho(r)$  (0.1560, 0.0666, & 0.0664 a.u.) and  $\rho(r)$  (0.0215, 0.0135 & 0.0134 a.u.) values respectively. According to this result, the

higher values of  $\nabla^2 \rho(r)$  &  $\rho(r)$  of R1 in comparison to the other two RCPs indicate the strongest repulsive steric effect in this aromatic ring, and it was confirmed by the RDG-NCI investigation.

# 3.2.2. LOL and ELF studies

Fig. 3 (a-d) shows color-filled and contour line maps of ELF and LOL of the chemical **4B2CA-LPA** respectively. A high value (or red color region) in that area denotes a strong localization of electrons caused by the presence of a nuclear shell [36]. In the present case, the maximum ELF regions are seen at H28 & H26 and show the localized electron bind between the atoms regions. The blue regions around a few atoms of chlorine and carbon atoms of Cl1, Cl2 & Cl1, show the delocalized electron cloud around it.

From Fig. 3(b) & (d), ELF & LOL contour map with gradient lines conveys a more definite and clearer picture of **4B2CA-LPA** whether the electron depletion region with dark blue circles at Cl1, & Cl2. Since the strongest delocalization regions are around Cl1-C17-C10 and Cl2-C18-C11 and they are visualized in Fig. 4 (a & b) respectively.

#### 3.2.3. RDG-NCI analysis

The red peaks at 0.05 to 0.23 a.u. in Fig. 5 (a) demonstrate the existence of strong steric repulsion influences at the center of the aromatic ring of the title molecule, while the green spikes at closely -0.01 a.u. is a clear indication that the interactions of van der Waals forces between the atoms H28 & H38 and NH $_2$  increase the compound's stability. By demonstrating the strong attraction of two hydrogen-hydrogen interactions (H23...H27 and H25...H28) the dark green with slit blue color spikes at -0.016 a.u improve the compound's stability and significant biological affinity. Additionally, the existence of weak contacts was confirmed in this investigation by Fig. 5 (b), which shows circular slabs with colored green, red, and dark green with blue among the atoms

# 3.3. Vibrational assignment

Vibrational spectra have been used to identify the 4B2CA-LPA

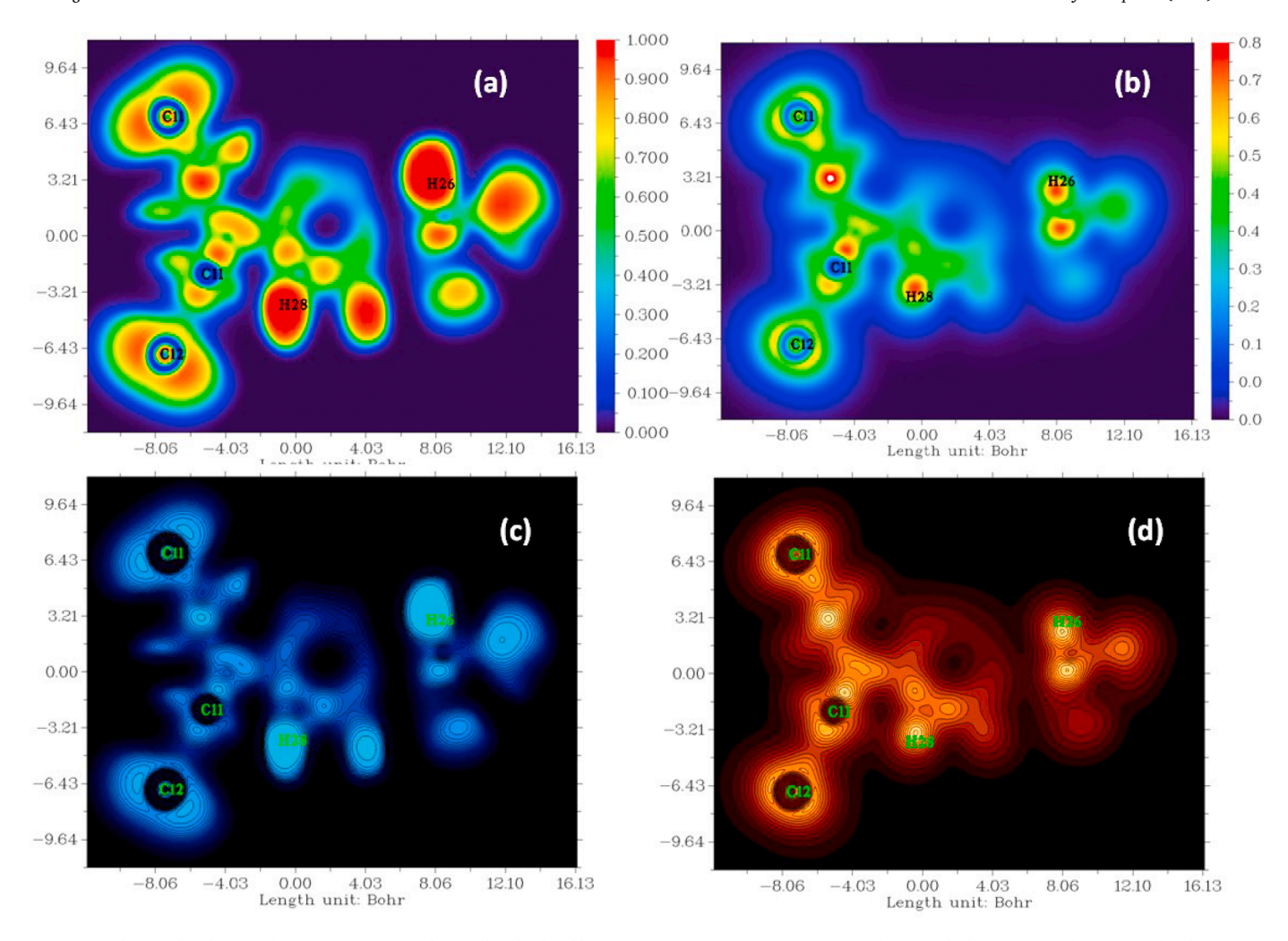


Fig. 3. (a) Electron localization function (ELF) map, (b) Localized orbital locator (LOL) map (c) contour surface of ELF, and (d) contour surface of LOL for the 4B2CA-LPA in the gas phase.

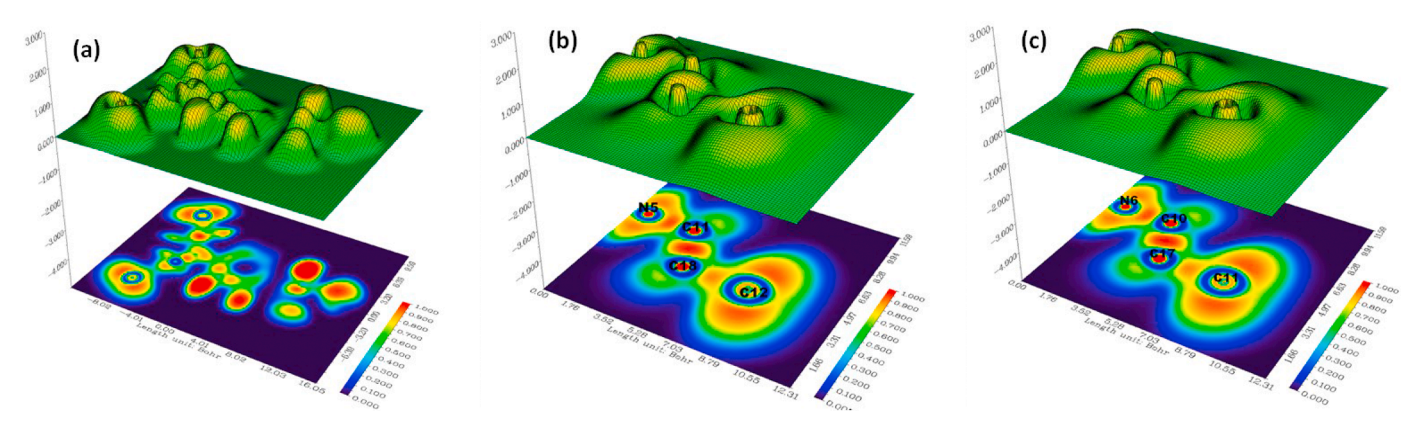


Fig. 4. The ELF map with an electronic environment shows that the highest delocalization region (a) entire molecule (b) Cl2-C18-C11 (c) Cl1-C17-C10 of 4B2CA-LPA.

molecule's functional groups in this study. For gaseous phases with the same optimization basis level, theoretical Raman and IR spectra of **4B2CA-LPA** were calculated [37,38] and are shown in Fig. 6. The molecule has 37 atoms and 45 normal modes of fundamental vibrations. The calculated vibrational frequencies were scaled using a scaling factor of 0.96 for all unscaled wavenumbers of 3744 to 18 cm $^{-1}$  [25], and the corresponding assignment with PED values is given in Table 3.

The different modes of OH stretching vibrations generally appear

between 3200 and 3650 cm $^{-1}$ [39]. In this case, the calculated IR spectrum bands in the molecule identified at 3594 cm $^{-1}$  and have 100% PED (mod no. 105) contribution. NH stretching typically varies from 3500 to 34000 cm $^{-1}$ [40]. The N6-H36 & N6-H35 atoms, which have 3438, and 3357 cm $^{-1}$  and a potential energy distribution of 100% for both (mode no. 103 & 104) are the cause of the stretching vibration of the amine (NH<sub>2</sub>). Typically, the functional group C=O arises between 1850 and 1550 cm $^{-1}$ . [41]. In this instance, the carbon atom C19

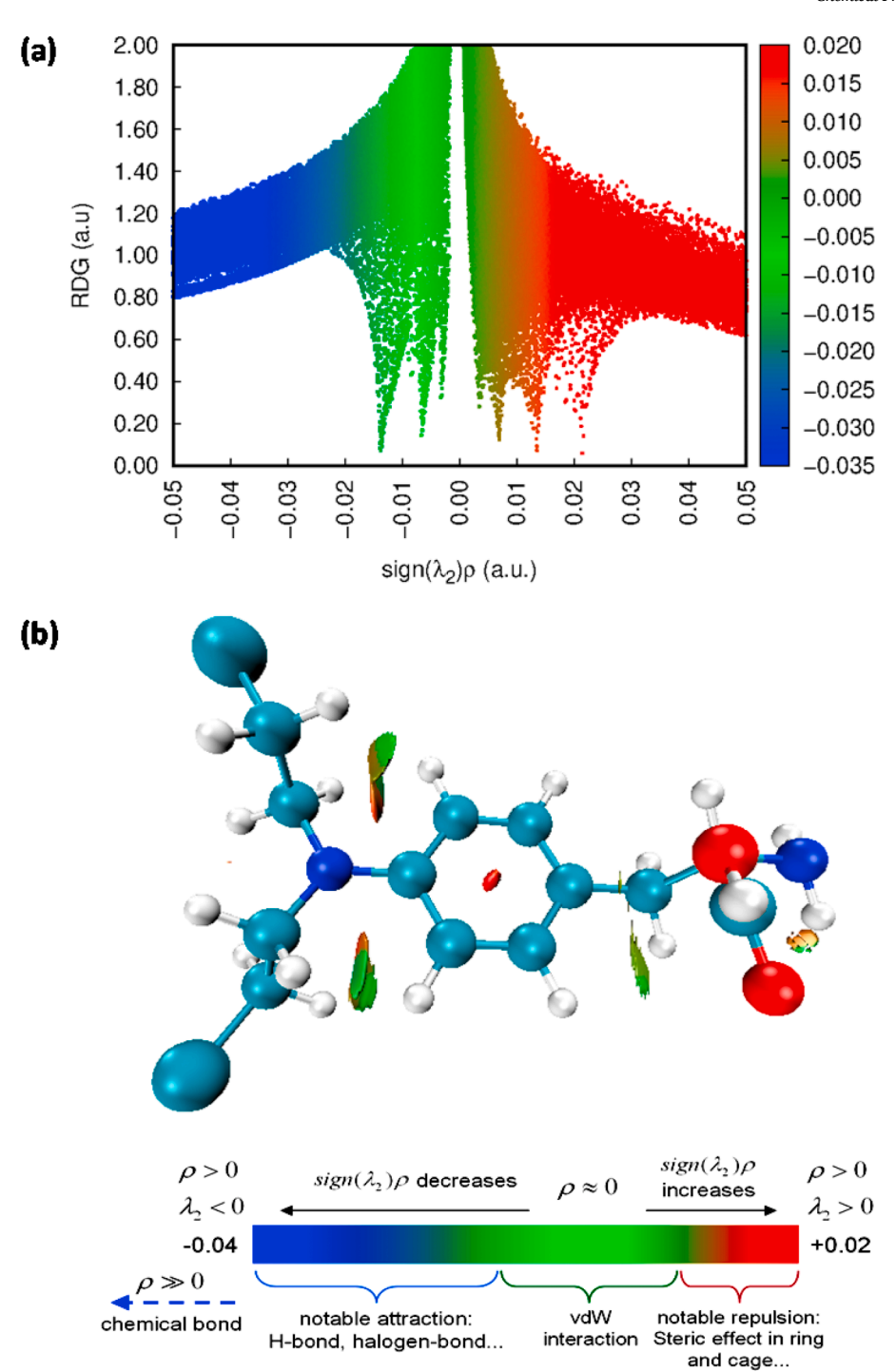


Fig. 5. RDG Plots versus the electron density  $\rho$  multiplied by the sign of  $\lambda_2$  of the title compound in the gas phase.

produced a double bond with the oxygen atom O4 at a current stretching vibration of  $1735~{\rm cm}^{-1}$  with a contribution from PED of 82% (mode no. 87). In vibrational analysis, the C-O stretching phase was usually found between 1180 and 989 cm $^{-1}$ . With maximum PED 56%, **4B2CA-LPA** (CO) stretching was seen at 1153, 1104, 1033 & 991cm $^{-1}$  (mode no. 59, 56, 53, & 51).

Aromatic compounds exhibit C-H stretching vibrations between 3000 and 3100 cm $^{-1}$  and 3280 and 3340 cm $^{-1}$  [42,43]. In this work, these vibrations were found at 3074, 3073, & 3036 cm $^{-1}$  with PED contribution 100% for all (mode no. 102-100). The CH<sub>2</sub> stretching was also found at 3029, 3028, 3026, 2973, 2971, 2968, 2967, 2961, 2943, 2936, and 2928 cm $^{-1}$  with PED contributions 100%, 100%, 52%, 98%,

100%, 100%, 57%, 57%, 100%, 100% (mode no. 99-88). The C-C harmonic stretching in aromatic compounds between 1650 and 800  $\rm cm^{-1}$  has been reported [44].

Evidence of possible  $C=C_{ring}$  stretching in this title molecule at 1441, 1428, 1181, 987, & 984 cm $^{-1}$  with PED contribution of 56%, 58%, 33%, 45%, & 52% (mode no. 81, 80, 61, 50 & 49) was calculated. The actual C-C-C bending vibrations mode has drawn attention in this study, and the maximum PED for CC vibrations is predicted to be 46%. Although stretching harmonics (CH) also contribute, their effects are less noticeable than those of (CC). These have a smaller PED rapport but influence C-C stretching. It follows that molecule vibrating modes were not at all affected by other vibrational modes since all reasonable frequency

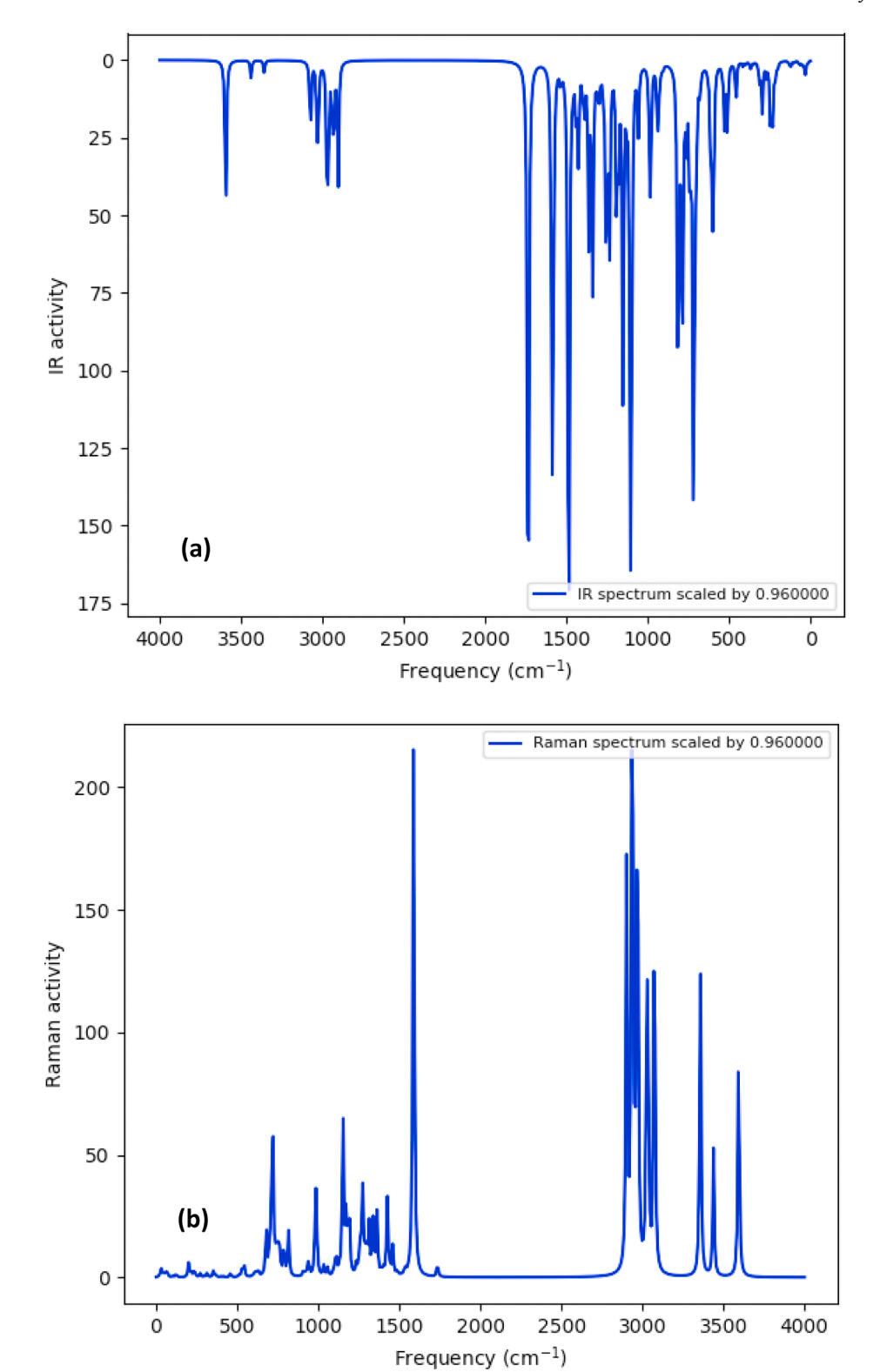


Fig. 6. Theoretical spectra of (a) IR spectrum (b) Raman spectrum of 4B2CA-LPA.

modes remained within the most expected range.

The C-N vibrations can be seen between 1670 and 1600 cm $^{-1}$ [45], but in the presently calculated at 1255 & 1058 cm $^{-1}$  PED values are 62%, & 11% (modes no. 66 & 54). Since a reduction in molecular symmetry and the presence of heavy atoms on the material's 4B2CA-LPA enable frequency coupling possible, it is important to take into account the vibrations associated with the link between the carbon atoms of two

 ${\rm CH_2}$  and two halogen atoms (Cl) in this situation. Usually, wide bands are produced by the C-Cl stretching mode in the range of 710-505 cm $^{-1}$  and this case at 702 & 679 cm $^{-1}$  with PED values of 40%, & 41% (mode no. 33 & 32).

Vibrational Assignment [%

**Table 3** Vibrational frequencies (cm $^{-1}$ ) with assignment, IR intensities (I $_{\rm IR}$ ; km mol $^{-1}$ ), Raman scattering activities (SA $_{\rm Raman}$ ; A $^4$ amu $^{-1}$ ) of 4B2CA-LPA were calculated using B3LYP/6-311++G(d,p) basis set in the gas phase.

| using B3    | LYP/6-311-           | ++G(d,p)     | basis set i     | n the gas p         | hase.      |  | 1101       |                               |                 |                |                     |          | PED] <sup>b</sup>  |
|-------------|----------------------|--------------|-----------------|---------------------|------------|--|------------|-------------------------------|-----------------|----------------|---------------------|----------|--|
| Mode<br>no. | DFT/B3LY             | P/6-311+-    | +G(d,p)         |                     |            | Vibrational<br>Assignment [%                                       |            | Freq.<br>Unscale <sup>a</sup> | Freq.<br>Scaled | $I_{IR}$       | SA <sub>Raman</sub> |          |  |
|             | Freq.                | Freq.        | $I_{IR}$        | SA <sub>Raman</sub> |            | PED] <sup>b</sup>  | 59         | 1201                          | 1153            | 119.07         | 69.63               | 59       | υCO(22)+βHCO<br>(24)   |
|             | Unscale <sup>a</sup> | Scaled       |                 |                     |            |  | 58         | 1176                          | 1129            | 10.48          | 2.17                | 58       | CH <sub>2</sub> wag(66)+βCH (38)                                     |
| 105<br>104  | 3744<br>3582         | 3594<br>3438 | 55.42<br>5.71   | 106.46<br>52.77     | 105<br>104 | υΟΗ(100)<br>υ <sub>asy</sub> NH <sub>2</sub> (100)                 | 57         | 1157                          | 1111            | 38.72          | 8.90                | 57       | $CH_2$ wag(58)+ $\beta$ NH   |
| 103         | 3497                 | 3357         | 4.28            | 134.11              | 103        | $v_{sy}NH_2(100)$  | 56         | 1150                          | 1104            | 174.89         | 1.83                | 56       | (39)<br>υCO(14)+βHCC   |
| 102         | 3202                 | 3074<br>3073 | 11.39           | 135.81              | 102        | $v_{\text{ring}}\text{CH}(100)$<br>$v_{\text{ring}}\text{CH}(100)$ | 30         | 1130                          | 1104            | 1/4.09         | 1.05                | 30       | (10)   |
| 101<br>100  | 3201<br>3162         | 3036         | 13.83<br>8.67   | 41.71<br>60.93      | 101<br>100 | υ <sub>ring</sub> CH(100)<br>υ <sub>ring</sub> CH(100)             | 55         | 1140                          | 1095            | 14.78          | 1.97                | 55       | βСОН(68)+βСН   |
| 99          | 3155                 | 3029         | 9.93            | 15.43               | 99         | $v_{\rm asy} CH_2(100)$  | <b>5</b> 4 | 1100                          | 1050            | 01.05          | 0.45                | -4       | (24)   |
| 98          | 3154                 | 3028         | 0.79            | 35.79               | 98         | $v_{asy}CH_2(99)$  | 54         | 1102                          | 1058            | 21.35          | 3.45                | 54       | υCN(11)+τHCCC<br>(10)  |
| 97          | 3152                 | 3026         | 19.02           | 70.42               | 97         | $v_{ring}CH$ (46)+ $v_{asy}CH_2(52)$                               | 53         | 1076                          | 1033            | 0.04           | 4.30                | 53       | υCO(19)+βHCO   |
| 96          | 3097                 | 2973         | 2.21            | 80.08               | 96         | $v_{sy}CH_2(100)$  | 52         | 1033                          | 991             | 10.21          | 1.92                | 52       | (16)<br>CH <sub>2</sub> wag(55)+βCH                                  |
| 95<br>94    | 3095<br>3091         | 2971<br>2968 | 32.72<br>11.89  | 6.02                | 95<br>94   | $v_{sy}CH_2(100)$  | 32         | 1033                          | JJ1             | 10.21          | 1.72                | 52       | (33)   |
| 93          | 3091                 | 2968<br>2967 | 2.37            | 95.49<br>34.13      | 93         | $v_{sy}CH_2(98)$<br>$v_{asy}CH_2(100)$                             | 51         | 1031                          | 990             | 0.63           | 11.87               | 51       | υCO(56)+βNH  |
| 92          | 3085                 | 2961         | 19.18           | 16.83               | 92         | υCH  |            |                               |                 |                |                     |          | (32)+βCH(11)   |
| 91          | 3065                 | 2943         | 2.39            | 73.64               | 91         | (41)+υ <sub>asy</sub> CH <sub>2</sub> (57)<br>υCH                  | 50         | 1028                          | 987             | 1.97           | 0.38                | 50       | υC=C(45)+βCH<br>(26)   |
|             |                      |              |                 |                     |            | $(41) + v_{asy}CH_2(57)$   | 49         | 1025                          | 984             | 29.57          | 25.99               | 49       | υC=C(52)+βNH (22)+βCH(36)  |
| 90          | 3059                 | 2936         | 16.11           | 227.67              | 90         | $v_{\rm sy}{\rm CH_2}(100)$  | 48         | 1023                          | 982             | 15.00          | 6.72                | 48       | $\beta_{\rm o} CH_{\rm ring}(32)$                                    |
| 89          | 3050                 | 2928         | 18.51           | 15.83               | 89         | υ <sub>sy</sub> CH <sub>2</sub> (100)                              | 47         | 980                           | 940             | 24.95          | 6.86                | 47       | $\beta_0 \text{CH}_{\text{ring}}(28)$                                |
| 88<br>87    | 3024<br>1808         | 2903<br>1735 | 40.78<br>251.78 | 170.80<br>5.87      | 88<br>87   | υ <sub>sy</sub> CH <sub>2</sub> (100)<br>υC=O(82)                  | 46         | 968                           | 929             | 5.44           | 0.67                | 46       | $\beta CCC_{ring}(50) + \beta CH$                                    |
| 86          | 1655                 | 1589         | 129.38          | 237.40              | 86         | υCC(68)+βHCC   |            |                               |                 |                |                     |          | (29)   |
|             |                      |              |                 |                     |            | (20)   | 45         | 962                           | 924             | 1.08           | 1.12                | 45       | CH <sub>3</sub> rock(32)   |
| 85          | 1646                 | 1580         | 50.90           | 5.88                | 85         | βНΝН(33)+βНСС  | 44         | 947                           | 909             | 1.99           | 2.59                | 44       | $\beta_0 \text{CH}_{\text{ring}}(56)$                                |
|             |                      |              |                 |                     |            | (21)   | 43<br>42   | 851<br>842                    | 817<br>809      | 75.75<br>52.86 | 18.03<br>1.40       | 43<br>42 | $\beta_{o}CH_{ring}(32)$<br>$\beta_{o}CH_{ring}(28)+CH_{2}$          |
| 84          | 1600                 | 1536         | 5.62            | 2.65                | 84         | υCC(68)+βHCO<br>(22)   |            |                               |                 |                |                     |          | rock(32)   |
| 83          | 1548                 | 1486         | 250.81          | 2.07                | 83         | vCC(80)+βHCC   | 41         | 822                           | 789             | 94.06          | 12.87               | 41       | CH <sub>2</sub> rock(53)   |
|             |                      |              |                 |                     |            | (10)   | 40<br>39   | 817<br>796                    | 785<br>764      | 13.19<br>24.82 | 0.43<br>5.21        | 40<br>39 | CH <sub>3</sub> rock(56)<br>$\nu$ CO(44)+βHCC                        |
| 82          | 1521                 | 1460         | 2.43            | 12.47               | 82         | βHNH(36)+βHCC<br>(51)  |            |                               |                 |                |                     |          | (10)   |
| 81          | 1501                 | 1441         | 16.11           | 1.87                | 81         | $vC=C_{ring}(56)+\beta CH$   | 38         | 788                           | 757             | 0.66           | 12.91               | 38       | CH <sub>2</sub> rock(58)   |
| 80          | 1488                 | 1428         | 8.56            | 15.31               | 80         | (22)+βNH $(20)vC=C_{ring}(58)+βCH$                                 | 37         | 775                           | 744             | 13.74          | 3.58                | 37       | $\beta_{o}$ CH <sub>ring</sub> (12)+ $\beta$<br>CHH(25)              |
|             |                      |              |                 |                     |            | (18)   | 36         | 772                           | 741             | 32.42          | 8.91                | 36       | $\beta_{\text{o}}\text{CH}_{\text{ring}}(28) + \beta \text{CH}$ (18) |
| 79          | 1486                 | 1426         | 17.24           | 11.12               | 79         | CH <sub>2</sub> scis(67)   | 35         | 752                           | 721             | 87.94          | 31.14               | 35       | $\beta_{\rm o} \text{CH}_{\rm ring}(19)$                             |
| 78<br>77    | 1484<br>1460         | 1424<br>1401 | 6.29<br>4.77    | 8.76<br>2.44        | 78<br>77   | CH <sub>2</sub> scis(77)<br>CH <sub>2</sub> scis (78)              | 34         | 747                           | 717             | 87.37          | 44.20               | 34       | CH <sub>3</sub> rock   |
| 77<br>76    | 1448                 | 1390         | 17.83           | 1.93                | 76         | CH <sub>2</sub> scis(37)   |            |                               |                 |                |                     |          | $(28)+\beta_o CH_{ring}(21)$   |
| 75          | 1420                 | 1363         | 56.55           | 25.64               | 75         | $CH_2twist(32)+\beta CH$   | 33         | 732                           | 702             | 31.82          | 13.89               | 33       | υCCl(40)+βHNH<br>(36)+βHCC(21)                                       |
| 74          | 1395                 | 1340         | 72.14           | 21.54               | 74         | (56)<br>CH <sub>3</sub> twist(28)+βCH                              | 32         | 708                           | 679             | 7.65           | 19.98               | 32       | υCCl(41)+βHNH  |
| 74          | 1393                 | 1340         | /2.14           | 21.54               | /4         | (29)   |            |                               |                 |                |                     |          | (48)+βHCC(18)  |
| 73          | 1389                 | 1333         | 4.73            | 3.13                | 73         | CH <sub>2</sub> twist(40)  | 31         | 656                           | 629             | 1.32           | 2.89                | 31       | $\beta$ CCC <sub>ring</sub> (68)+ $\beta$                            |
| 72          | 1368                 | 1314         | 2.84            | 21.03               | 72         | CH <sub>2</sub> twist(38)  | 30         | 639                           | 613             | 38.79          | 2.46                | 30       | CNH(21)<br>βNH(18)+βCH(70)   |
| 71          | 1357                 | 1302         | 12.49           | 4.37                | 71         | β <sub>i</sub> CH <sub>ring</sub> (28)                             | 29         | 623                           | 598             | 65.54          | 0.70                | 29       | βNH(11)+βCH(80)  |
| 70          | 1348                 | 1294         | 2.81            | 11.84               | 70         | $CH_2$ twist(29)+ $\beta$ CH (46)                                  | 28         | 565                           | 542             | 1.54           | 5.60                | 28       | $\beta$ HCN(60)+ $\beta$ NH  |
| 69          | 1328                 | 1275         | 4.68            | 34.98               | 69         | βNCO(62)+βCH<br>(23)   | 27         | 552                           | 529             | 20.22          | 2.70                | 27       | (11)<br>NH <sub>2</sub> wag(68)+βOH                                  |
| 68          | 1317                 | 1265         | 4.33            | 8.05                | 68         | CH <sub>2</sub> wag(78)  |            |                               |                 |                |                     |          | (22)   |
| 67          | 1310                 | 1258         | 4.44            | 4.60                | 67         | $CH_2$ wag(48)+ $\beta$ CH<br>(29)+ $\beta$ NCO(10)                | 26         | 532                           | 511             | 23.93          | 0.79                | 26       | βCH(12)+βNHH<br>(60)   |
| 66          | 1307                 | 1255         | 68.25           | 6.20                | 66         | υCN(62)+βCH  | 25         | 478                           | 459             | 13.06          | 1.60                | 25       | βCOH(12)+βCNC<br>(48)  |
| 65          | 1288                 | 1237         | 28.50           | 2.62                | 65         | (32)+βNCO $(26)CH2wag(87)+βCH$                                     | 24         | 434                           | 416             | 1.49           | 0.35                | 24       | CH <sub>2</sub> rock(23)+β<br>CH <sub>ring</sub> (22)                |
| 64          | 1287                 | 1235         | 36.04           | 2.23                | 64         | (11)<br>CH <sub>2</sub> wag(59)+βCH                                | 23         | 416                           | 399             | 0.95           | 0.32                | 23       | NH <sub>2</sub> rock(78)+β   |
| 63          | 1243                 | 1194         | 35.24           | 1.87                | 63         | (12)<br>βCH(26)+βCCO   | 22         | 386                           | 370             | 2.40           | 0.71                | 22       | COH(11)<br>NH <sub>2</sub> rock(68)+ $\beta$                         |
|             |                      |              |                 |                     |            | [28]   | 21         | 369                           | 354             | 0.78           | 2.86                | 21       | COH(32)<br>NH <sub>2</sub> rock(58)+β                                |
| 62          | 1241                 | 1191         | 11.13           | 26.30               | 62         | βCCC(28)+βCH<br>(12)   |            |                               |                 |                |                     |          | COH(12)  |
| 61          | 1230                 | 1181         | 33.62           | 7.53                | 61         | CH <sub>2</sub> twist(62)+ $\upsilon$<br>C=C <sub>ring</sub> (33)  | 20         | 328                           | 314             | 6.88           | 1.78                | 20       | $\beta CH_{ring}(20) + \beta$ $CHHC(16)$                             |
| 60          | 1220                 | 1172         | 0.78            | 22.86               | 60         | CH <sub>2</sub> rock(48)+βCH                                       | 19         | 309                           | 297             | 16.24          | 0.28                | 19       | βCNC(58)+βCOH<br>(22)  |
|             |                      |              |                 |                     |            | (18)   |            |                               |                 |                |                     | ,        | (44)   |

Table 3 (continued)

DFT/B3LYP/6-311++G(d,p)

Mode

no.

(continued on next page)

Table 3 (continued)

| Mode<br>no. | DFT/B3LY                      | P/6-311++       |          | Vibrational<br>Assignment [%<br>PED] <sup>b</sup> |    |  |
|-------------|-------------------------------|-----------------|----------|---|----|--|
|             | Freq.<br>Unscale <sup>a</sup> | Freq.<br>Scaled | $I_{IR}$ | SA <sub>Raman</sub>                               |    | 1 110]   |
| 18          | 284                           | 272             | 4.23     | 1.51  | 18 | βCCO(54)+β<br>CHring(18)                                     |
| 17          | 258                           | 247             | 18.64    | 0.17  | 17 | βHCCH(40)+βOCO (20)  |
| 16          | 248                           | 238             | 9.78     | 1.60  | 16 | $\beta$ CO(44)+ $\beta$<br>CH <sub>ring</sub> (15)           |
| 15          | 242                           | 233             | 14.19    | 1.37  | 15 | βCCC <sub>ring</sub> (58)+β<br>CCC(25)                       |
| 14          | 228                           | 219             | 3.53     | 1.00  | 14 | βCCH(42)+βCNO<br>(17)  |
| 13          | 222                           | 213             | 1.93     | 1.31  | 13 | $\beta CH_{ring}(42)$  |
| 12          | 209                           | 201             | 1.37     | 5.73  | 12 | βCO(48)+β  |
| 11          | 136                           | 131             | 0.92     | 0.31  | 11 | $CH_{ring}(28)$<br>$\beta CO(38) + \beta$<br>$CH_{ring}(28)$ |
| 10          | 127                           | 122             | 1.91     | 1.04  | 10 | $\beta CH_2(22) + \beta$ $CH_{ring}(10)$                     |
| 9           | 106                           | 102             | 0.66     | 0.45  | 9  | βCCN(28)+βCNH<br>(22)  |
| 8           | 74                            | 71              | 0.71     | 1.21  | 8  | $\beta$ CO(21)+ $\beta$ CH <sub>ring</sub> (47)              |
| 7           | 64                            | 61              | 1.30     | 2.25  | 7  | βCCC <sub>ring</sub> (68)                                    |
| 6           | 51                            | 49              | 0.72     | 1.00  | 6  | βCH(15)+βOH(12)  |
| 5           | 37                            | 36              | 0.38     | 1.45  | 5  | βCNH(11)+β<br>CH <sub>ring</sub> (13)                        |
| 4           | 35                            | 34              | 4.43     | 0.89  | 4  | $\beta CO(25) + \beta$                                       |
| 3           | 32                            | 31              | 0.36     | 1.81  | 3  | $CH_{ring}(22)$<br>$\beta CCN(34) + \beta CNH$               |
| 2           | 25                            | 24              | 0.21     | 0.26  | 2  | (12)<br>βCHC <sub>ring</sub> (38)+β                          |
| 1           | 18                            | 17              | 0.55     | 0.25  | 1  | COH(26)<br>βCCN(11)+βCNH<br>(22)                             |

<sup>&</sup>lt;sup>a</sup> [Scaling factors of 0.96 are used to scale down calculated wavenumbers for all frequencies]

### 3.4. FMOs analysis: HOMO-LUMO energy prediction

The 4B2CA-LPA molecule's pharmacokinetics and stabilization can be understood by using energy values of filled and empty orbitals (HOMO & LUMO). Soft chemicals are compounds with a narrow FMO band gap and high chemical excitability [46]. To explore 4B2CA-LPA better, the effect of the solution was studied in this instance. Fig. 7 and Table 4 provide an understanding of the spectral gap ( $\Delta E$ ) with different solvents. The band gap energies of various solvents are 4.9781, 4.9441, 4.9463, and 4.9420 eV, whereas the chemical potential differences in solvents are -3.1808, -3.1630, -3.1635, and -3.1627 eV (for chloroform, DMSO, methanol, and water, respectively) indicating that the molecule is significantly more reactive in water compared to other solutions. This was determined by the discovery of the minimum energy in the water phase. For chloroform, DMSO, methanol, and water, respectively, the softness energies are 0.2009, 0.2023, 0.2022, and 0.2023 eV; the hardness 2.4891, 2.4721, 2.4732, & 2.4710 eV. Since the 4B2CA-LPA was less harmful in these phases because DMSO and water had the highest levels of softness and minimal hardness, demonstrating the compound's good biological properties.

# 3.5. MEP analysis

The MEP prediction predicted the comparative reactivity sites of a molecule for electrophilic and nucleophilic attacks [47]. Employing the optimized structure was used to calculate the MEP surface analysis in gas and various solvent of chloroform, DMSO, methanol, and water of the 4B2CA-LPA. Fig. 8 shows the mapped ESP surface of the investigated chemical 4B2CA-LPA. The position of nucleophilic, and electrophilic assaults concerning the colors of blue, and red in the range from +100.00 to -100.00 in Fig. 8.

The MEP results indicate that on the surface of molecules, 14 surface maxima (positive values) and 7 surface minima (negative values) were acquired in all phases. The more negative values or minimum electrostatic energies were found at  $NH_2$  (-32.845, 35.34, -36.52, -36.45 & -36.58 kcal/mol) and O4 (-19.115, -34.31, -35.55, -35.49 & -35.62 kcal/ mol) regions with red color regions in gas, chloroform, DMSO, methanol, and water respectively. The maximum electrostatic energies or more positive values were found at CH2 (C8-H20-H-21; 48.642, 51.77, 52.90, 52.85 & 52.95 kcal/mol) with blue regions in gas, chloroform, DMSO, methanol, and water respectively. Since this result shows that the maximum possibility of a strong nucleophilic attack region is NH<sub>2</sub> and among the solvents, water has the highest energy -36.58 kcal/mol compared to other solvents, whereas the maximum possibility of the strongest electrophilic attack region is CH2 (C8-H20-H-21) and among the solvent, the solvent water has the highest energy 52.95 kcal/mol compared to other solvents.

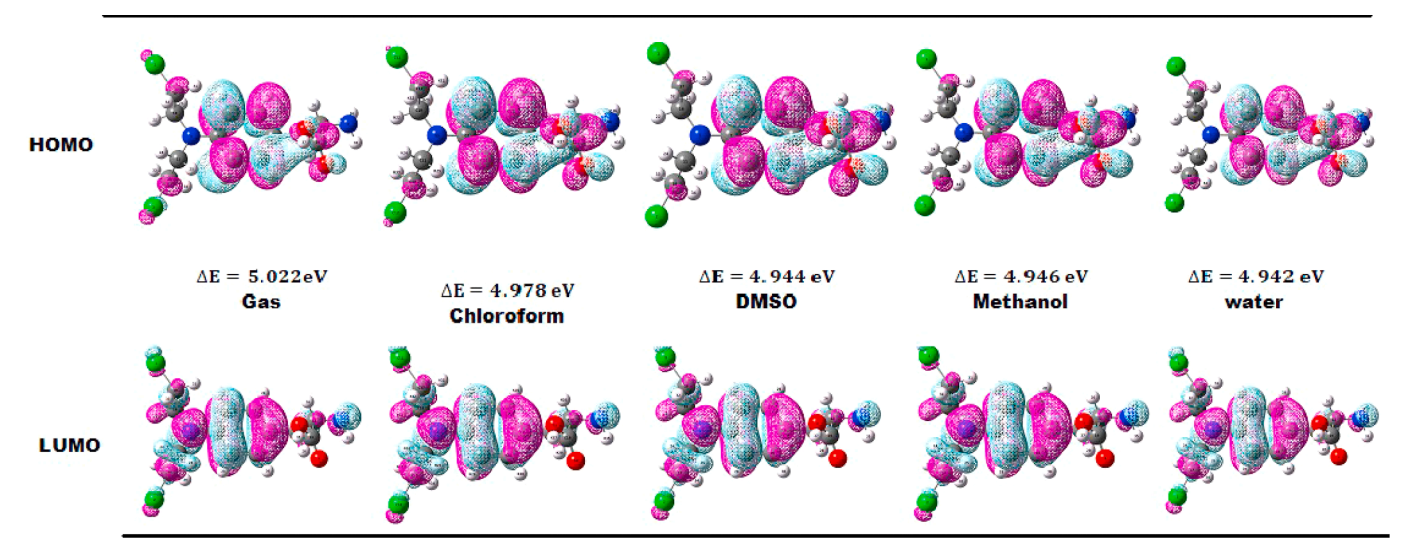


Fig. 7. The Frontier molecular orbitals (HOMOs & LUMOs) in the gas and solvent phases of the title compound.

 $<sup>^</sup>b$  [% PED- Percentage of potential energy distribution;v-stretching,  $\upsilon_{sy}\text{-symmetric}$  stretching,  $\upsilon_{asy}\text{-asymmetric}$  stretching,  $\beta\text{-bending}$ , scis-scissoring, wagwagging, twist-twisting, rock-rocking &  $\tau$ - torsion].

Table 4 Calculated Frontier Molecular Orbital (FMO) energy parameters (all in eV) highest occupied molecular orbital energy ( $E_{HOMO}$ ), lowest unoccupied molecular orbital energy ( $E_{LUMO}$ ), Energy gap ( $\Delta E_g$ ), Ionization potential ( $I_P$ ), Electron affinity ( $E_a$ ), chemical hardness ( $\eta$ ), chemical softness (S), electro negativity ( $\chi$ ), chemical potential ( $\mu$ ), and electrophilicity index ( $\omega$ ) of the title compound in different mediums.

| Medium     | $E_{\text{HOMO}}$ | $E_{LUMO}$ | ΔΕ    | $I_P$  | Ea     | η      | S      | χ      | μ       | ω      |
|------------|-------------------|------------|-------|--------|--------|--------|--------|--------|---------|--------|
| Gas        | -5.8175           | -0.7956    | 5.022 | 5.8175 | 0.7956 | 2.5110 | 0.1991 | 3.3066 | -3.3066 | 2.1771 |
| Chloroform | -5.6698           | -0.6917    | 4.978 | 5.6698 | 0.6917 | 2.4891 | 0.2009 | 3.1808 | -3.1808 | 2.0323 |
| DMSO       | -5.6350           | -0.6909    | 4.944 | 5.6350 | 0.6909 | 2.4721 | 0.2023 | 3.1630 | -3.1630 | 2.0235 |
| Methanol   | -5.6367           | -0.6903    | 4.946 | 5.6367 | 0.6903 | 2.4732 | 0.2022 | 3.1635 | -3.1635 | 2.0233 |
| Water      | -5.6337           | -0.6917    | 4.942 | 5.6337 | 0.6917 | 2.4710 | 0.2023 | 3.1627 | -3.1627 | 2.0240 |

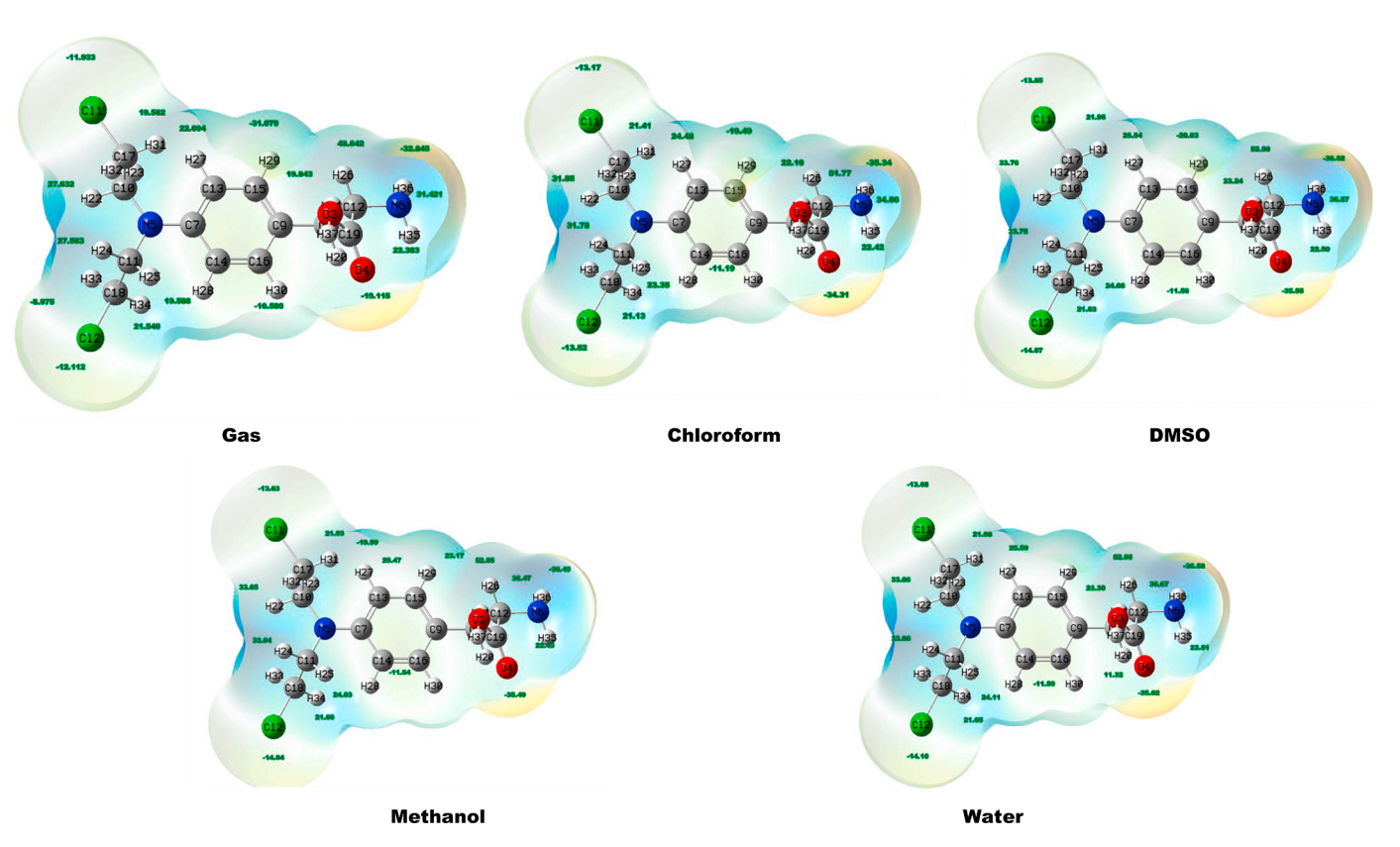


Fig. 8. Molecular Electrostatic Potential (MEP) surface map of 4B2CA-LPA in gas and different solvents phases.

 $\begin{tabular}{ll} \textbf{Table 5} \\ \textbf{S-order perturbation theory of Fork matrix selected NBO analysis of title compound based on B3LYP/6-311++G(d,p) basis set. \\ \end{tabular}$ 

| Donor (i) | Acceptor (j) | Type of Transition | Occupancy | (ED/e)       | Energy E <sup>(2)a</sup> KJ/mol | Energy difference E(j)-E(i) <sup>b</sup> a.u | Polarized energy F(i,j) <sup>c</sup> a.u |
|-----------|--------------|--------------------|-----------|--------------|---------------------------------|--|--|
|           |              |                    | Donor (i) | Acceptor (j) |                                 |  |  |
| O3-C19    | C18-H34      | σ-σ*               | 1.99531   | 0.01951      | 141.6                           | 3.71   | 0.649                                    |
| O3-H37    | C18-H34      | σ-σ*               | 1.98695   | 0.01951      | 130.7                           | 3.50   | 0.605                                    |
| LP(n)N6   | C18-H34      | LP (n)-σ*          | 1.95124   | 0.01951      | 75.4                            | 3.00   | 0.428                                    |
| LP(n)Cl2  | C18-H34      | LP (n)-σ*          | 1.99713   | 0.01951      | 53.7                            | 3.61   | 0.395                                    |
| LP(n)O3   | O4-C19       | LP (n)-π*          | 1.81196   | 0.20186      | 49.6                            | 0.32   | 0.113                                    |
| LP(n)Cl2  | C18-H34      | LP (n)-σ*          | 1.97772   | 0.01951      | 40.1                            | 3.05   | 0.312                                    |
| LP(n)N5   | C7-C14       | LP (n)-π*          | 1.7435    | 0.42081      | 39.5                            | 0.27   | 0.097                                    |
| LP(n)O3   | C18-H34      | LP (n)-σ*          | 1.97666   | 0.01951      | 38.2                            | 3.41   | 0.322                                    |
| LP(n)O4   | O3-C19       | LP (n)-σ*          | 1.84924   | 0.0985       | 32.7                            | 0.62   | 0.129                                    |
| LP(n)O3   | C18-H34      | LP (n)-σ*          | 1.81196   | 0.01951      | 30.8                            | 3.08   | 0.287                                    |
| LP(n)O4   | C18-H34      | LP (n)-σ*          | 1.97839   | 0.01951      | 29.1                            | 3.44   | 0.283                                    |
| C9-C16    | C13-C15      | π-π*               | 1.6597    | 0.34599      | 23.7                            | 0.28   | 0.072                                    |
| C7-C14    | C9-C16       | π-π*               | 1.63867   | 0.37046      | 23.2                            | 0.29   | 0.074                                    |
| O3-H37    | C18-H33      | σ-σ*               | 1.98695   | 0.01966      | 22.0                            | 1.26   | 0.149                                    |

# 3.6. NBO analysis

The second-order Fock matrix was utilized in the NBO technique to assess the acceptor-donor interactions of 4B2CA-LPA [48]. The

calculated NBO parameters for **4B2CA-LPA** are listed in Table 5. From this table, the highest stabilization was found for the transition of  $\sigma\text{-}\sigma^*$  between the natural bonds of (O3-C19) and (C18-H34) with an energy value of 141.6 kJ/mol. And the next strongest transition identified for

Table 6 Electronic excitations of **4B2CA-LPA** obtained by experimental and TD-DFT/ B3LYP/6-311++G(d,p) method.

| Medium     | TD-DFT/                  | B3LYP/6-3              | 11++G(d,p)                    | )                          | Major   |
|------------|--------------------------|------------------------|-------------------------------|----------------------------|---|
|            | λ <sub>max</sub><br>(nm) | Band<br>gap ΔE<br>(eV) | Energy<br>(cm <sup>-1</sup> ) | Oscillator<br>Strength (f) | contribution <sup>a</sup>   |
| Gas        | 241.31                   | 5.139                  | 41441                         | 0.2608                     | $H \rightarrow L+1$ (28%), H<br>$\rightarrow L+2$ (23%), H<br>$\rightarrow L+3$ (16%), H<br>$\rightarrow L+9$ (14%) |
| Chloroform | 242.90                   | 5.105                  | 41169                         | 0.3975                     | $H \rightarrow L+1$ (36%), $H$<br>→ $L+2$ (10%), $H$<br>→ $L+3$ (10%), $H$<br>→ $L+9$ (25%)                         |
| DMSO       | 243.02                   | 5.102                  | 41149                         | 0.4135                     | $H \rightarrow L+1 (49\%), H$<br>$\rightarrow L+9 (24\%)$   |
| Ethanol    | 242.65                   | 5.110                  | 41212                         | 0.3951                     | $H \rightarrow L+ 1(50\%), H$<br>$\rightarrow L+9 (24\%)$   |
| Methanol   | 242.70                   | 5.109                  | 41203                         | 0.3951                     | $H \rightarrow L+ 1(50\%), H$<br>$\rightarrow L+9 (24\%)$   |
| Water      | 242.74                   | 5.108                  | 41196                         | 0.3984                     | $H \rightarrow L+ 1(50\%), H$<br>$\rightarrow L+9 (24\%)$   |

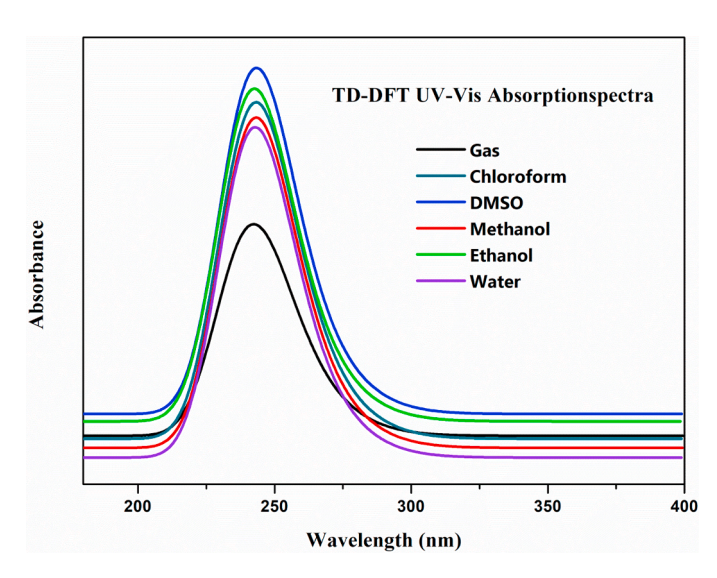


**Fig. 9.** The UV-Visible absorption spectrum of theoretical TD-DFT spectra for different mediums.

σ-σ\* between the natural bonds of (O3-H37) and (C18-H34) with an energy value of 130.7 kJ/mol. Interactions are largely caused by lone pairs of nitrogen, chlorine, and oxygen ions (e.g., N6, Cl2, O3, N5, O3, & O4) and anti-bonding σ\* and π\* groups with better interaction energies, which stated that the charge transfer among natural bonds and increase molecular stability. E.g. the lone pair transitions are LP(n)N6  $\rightarrow$  (C18-H34), LP(n)Cl2 $\rightarrow$ (C18-H34), LP(n)O3 $\rightarrow$ (C4-C19), LP(n)Cl2 $\rightarrow$ (C18-H34), LP(n)N5 $\rightarrow$ (C7-C14), LP(n)O3 $\rightarrow$ (C18-H34), LP(n)O4 $\rightarrow$ (O3-C19), LP(n)O3 $\rightarrow$ (C18-H34) and LP(n)O4 $\rightarrow$ (C18-H34) with energies are 75.4, 53.7, 49.6, 40.1, 39.5, 38.2, 32.7, 30.8, & 29.1 kJ/mol respectively.

#### 3.7. UV-Vis absorption studies

The electronic transition of 4B2CA-LPA was theoretically obtained with different solutions of chloroform, DMSO, ethanol, methanol, and water, as well as for the gaseous state, using the approach TD-DFT with the same basis set level. The findings are provided in Table 6 and shown in Fig. 9. The gas phase has the longest wavelength of 241.31 nm and energy of 5.139 eV which is greatly helped by the electronic absorption of 4B2CA-LPA from the frontier orbitals [49] with a 28% maximum contribution of HOMO-LUMO+1 transition. Among the solvent phases, the DMSO's lowest energy is 41149 cm<sup>-1</sup> with maximum wavelengths of 243.02 nm, respectively. Band gap values of chloroform, DMSO, ethanol, methanol, and water are 5.139, 5.105, 5.102, 5.110, 5.109, and 5.108 eV, respectively. This shows that the molecule in DMSO solvent has greater electronic characteristics and less kinetic stability.

#### 3.9. Molecular docking studies

Computerized drug design and basic molecular biology both have an advantage in the study of molecular docking [50]. The drug Alkeran is one of the most effective therapies for multiple myeloma currently available. Myeloma is often referred to as plasma cell cancer or blood cancer. Also based on PASSOnline tool prediction for **4B2CA-LPA**, the highest probability activity (Pa = 0.921) was found for Hematopoietic inhibitor and it is given in **Table S1 (supplementary file)**. Blood cell production is increased by hematopoietic drugs. The terms "hema" and "poiesis" both refer to blood. The generation of serum, or red blood cells, phagocytes, which are tiny pieces of a bigger cell called a megakaryocyte that forms clots, is particularly increased by hematopoietic medicines.

Since this investigation for **4B2CA-LPA**, we selected three different blood cell-related cancer proteins (PDB codes: 4FVR, 3WIX, & 5UUT) for molecular docking with the title chemical **4B2CA-LPA**. The focus of this research was to determine which of these three blood cancer cells had the best docking score with the greatest binding energy and the most residues in non-covalent interaction; (a) *4FVR*: Janus kinase 2 (JAK2) mutants V617F is a protein tyrosine kinase that regulates signaling via several cytokine receptors in blood cancer cells. (b) *3WIX*: The human myeloid leukaemia cell development protein (hMcl-1) is a number of coanti-apoptotic enzymes that belongs to the B-cell lymphoma-2 (Bcl-2) family proteins. it is a key pharmacological target in blood tumors. (c) *5UUT*: N-myristoyl-transferase 1 (NMT) protein is involved in the malignant progression of prostate cancer in blood cells and enables cell localization [51–53].

The Auto Dock software, which can find the optimal binding pose for Protein couplings, was used to execute this docking research. Binding characteristics including reference RMSD rate, binding energy, electrostatic energy, intramolecular energy, inhibit activity, and others are included in both Table 7 and Fig. 10.

As a docking result, the title compound **4B2CA-LPA** interacted well with all targeted proteins with good binding energy (-6.78, -7.30 & -5.10 kcal/mol) for proteins 4FVR, 3WIX, and 5UUT. The highest binding energy -7.30 kcal/mol with many weak interactions was found for *3WIX*: The human myeloid leukaemia cell development protein (hMcl-1) with the compound **4B2CA-LPA**. The Non-covalent weak interactions between 4B2CA-LPA and targeted proteins (a) 4FVR, (b) 3WIX, & (c) 5UUT

Table 7
Molecular docking results of binding energy (in kcal mol<sup>-1</sup>), inhibition constant (in μm), electrostatic energy (in kcal mol<sup>-1</sup>) intermolecular energy (in kcal mol<sup>-1</sup>), and RMSD values (in Å) for the compound **4B2CA-LPA** with three different proteins (PDB code: 4FVR, 3WIX & 5UUT).

| Protein (PDB code) | Type of organism | ligand<br>molecule | Binding affinity (Kcal $mol^{-1}$ ) | Inhibition constant<br>(μm) | Electrostatic energy (Kcal $\text{mol}^{-1}$ ) | Inter molecular energy (Kcal $mol^{-1}$ ) | Reference RMSD<br>(Å) |
|--------------------|------------------|--------------------|-------------------------------------|-----------------------------|--|---|-----------------------|
| 4FVR               | Homo sapiens     | 4B2CA-LPA          | -6.78                               | 311.57                      | -1.19  | -7.77                                     | 23.26                 |
| 3WIX               | Homo sapiens     | 4B2CA-LPA          | -7.30                               | 4.45                        | -0.87  | -10.28                                    | 55.92                 |
| 5UUT               | Homo sapiens     | 4B2CA-LPA          | -5.10                               | 181.31                      | -1.00  | -8.09                                     | 30.99                 |

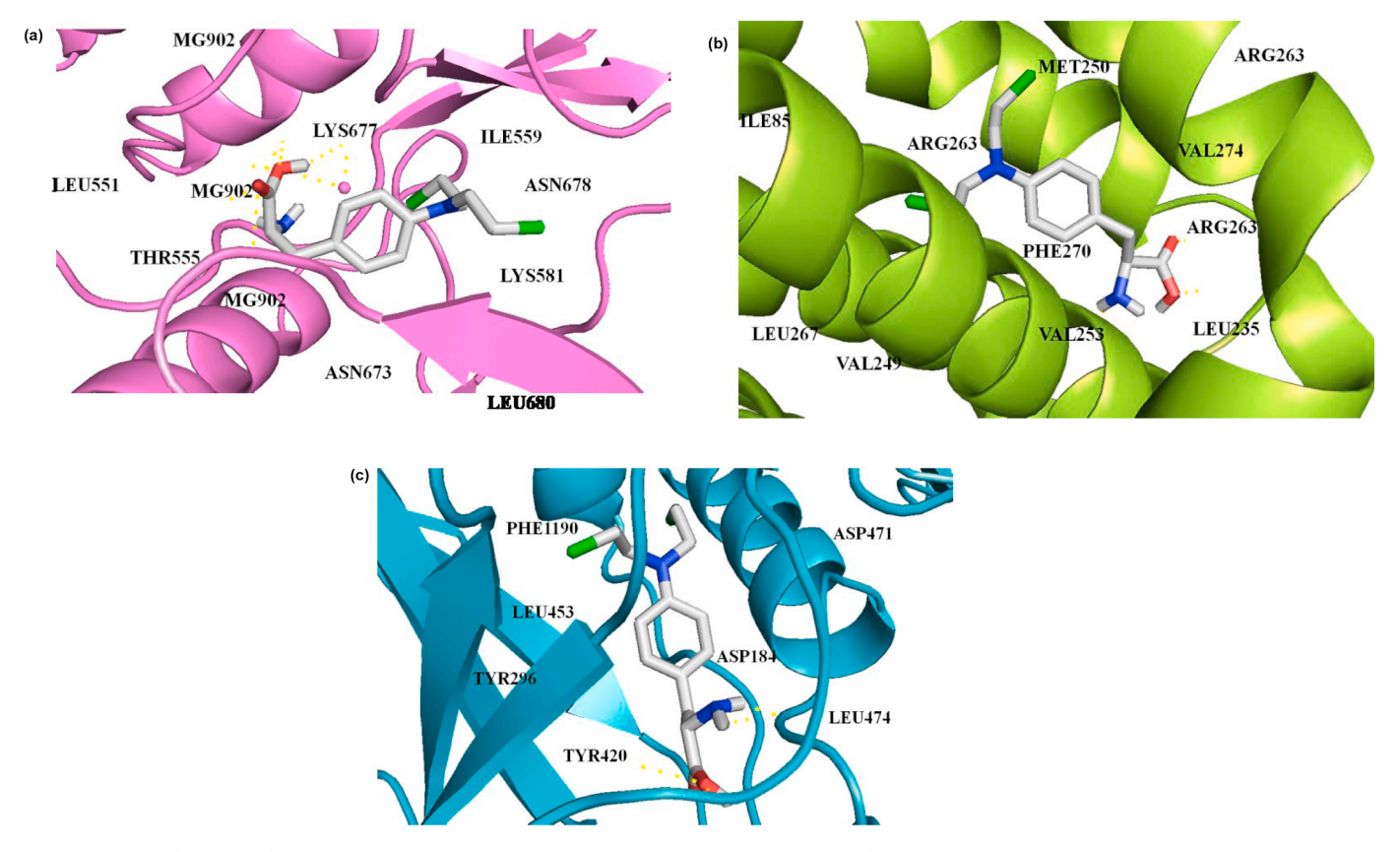


Fig. 10. The protein-ligand interaction surface with the best-docked pose of 4B2CA-LPA with targeted proteins (a) 4FVR, (b) 3WIX, & (c) 5UUT.

**Table 8**The Non-covalent weak interactions between the ligand 4B2CA-LPA and three different proteins 4FVR, 3WIX & 5UUT.

| Ligand    | Protein | Binding Energy (kcal $\mathrm{mol}^{-1}$ ) | Ligand group    | Protein Residues | *Type of interaction | Distance (Å |
|-----------|---------|--|-----------------|------------------|----------------------|-------------|
| 4B2CA-LPA | 4FVR    | -4.78                                      | C=O             | LYS677           | СОНВ                 | 5.63        |
|           |         |  | C=O             | THR555           | COHB                 | 3.93        |
|           |         |  | OH              | ASN678           | COHB                 | 4.39        |
|           |         |  | OH              | ASN673           | COHB                 | 4.86        |
|           |         |  | OH              | MG902            | UNMD                 | 2.03        |
|           |         |  | C-Cl            | MG902            | MAC                  | 5.47        |
|           |         |  | BEN             | LYS581           | PCA                  | 6.33        |
|           |         |  | BEN             | MG902            | PCA                  | 3.39        |
|           |         |  | BEN             | ILE559           | AKL                  | 5.47        |
|           |         |  | $CH_2$          | LEU680           | PAL                  | 5.2         |
|           |         |  | $CH_2$          | LEU551           | PAL                  | 4.8         |
| 4B2CA-LPA | 3WIX    | -7.30                                      | $NH_2$          | ARG263           | COHB                 | 4.76        |
|           |         |  | $NH_2$          | ARG263           | COHB                 | 4.04        |
|           |         |  | OH              | ARG263           | COHB                 | 2.21        |
|           |         |  | OH              | ARG263           | COHB                 | 3.67        |
|           |         |  | C=O             | ARG263           | COHB                 | 4.05        |
|           |         |  | BEN             | PHE270           | PPTS                 | 4.58        |
|           |         |  | $CH_2$          | ILE85            | AKL                  | 5.11        |
|           |         |  | $CH_2$          | VAL249           | AKL                  | 4.7         |
|           |         |  | CH <sub>2</sub> | LEU235           | AKL                  | 3.43        |
|           |         |  | CH <sub>2</sub> | MET250           | PAL                  | 4.58        |
|           |         |  | CH <sub>2</sub> | VAL274           | PAL                  | 5.5         |
|           |         |  | BEN             | LEU267           | PAL                  | 5.18        |
|           |         |  | BEN             | VAL253           | PAL                  | 6.39        |
| 4B2CA-LPA | 5UUT    | -5.10                                      | $NH_2$          | ASP184           | COHB                 | 4.1         |
|           |         |  | $NH_2$          | ASP471           | COHB                 | 3.77        |
|           |         |  | BEN             | PHE1190          | PPTS                 | 6.51        |
|           |         |  | $CH_2$          | LEU453           | AKL                  | 5.38        |
|           |         |  | $CH_2$          | TYR420           | AKL                  | 5.96        |
|           |         |  | $CH_2$          | LEU474           | PAL                  | 5.68        |
|           |         |  | CH <sub>2</sub> | TYR296           | PAL                  | 5.26        |

<sup>\* [</sup>COHB - Conventional Hydrogen bond; UFDD - Unfavourable Donor-Donor; AKL-Alkyl; PCA-  $\pi$ -Cation; PAN-  $\pi$ -Anion; PAL-  $\pi$ -Alkyl; PPS -  $\pi$ - $\pi$  Stack; PPTS-  $\pi$ - $\pi$  T shaped; APS- Amide  $\pi$ -stacked; UNMD- Unfavourable Metal-Donor; MAC- Metal Acceptor]

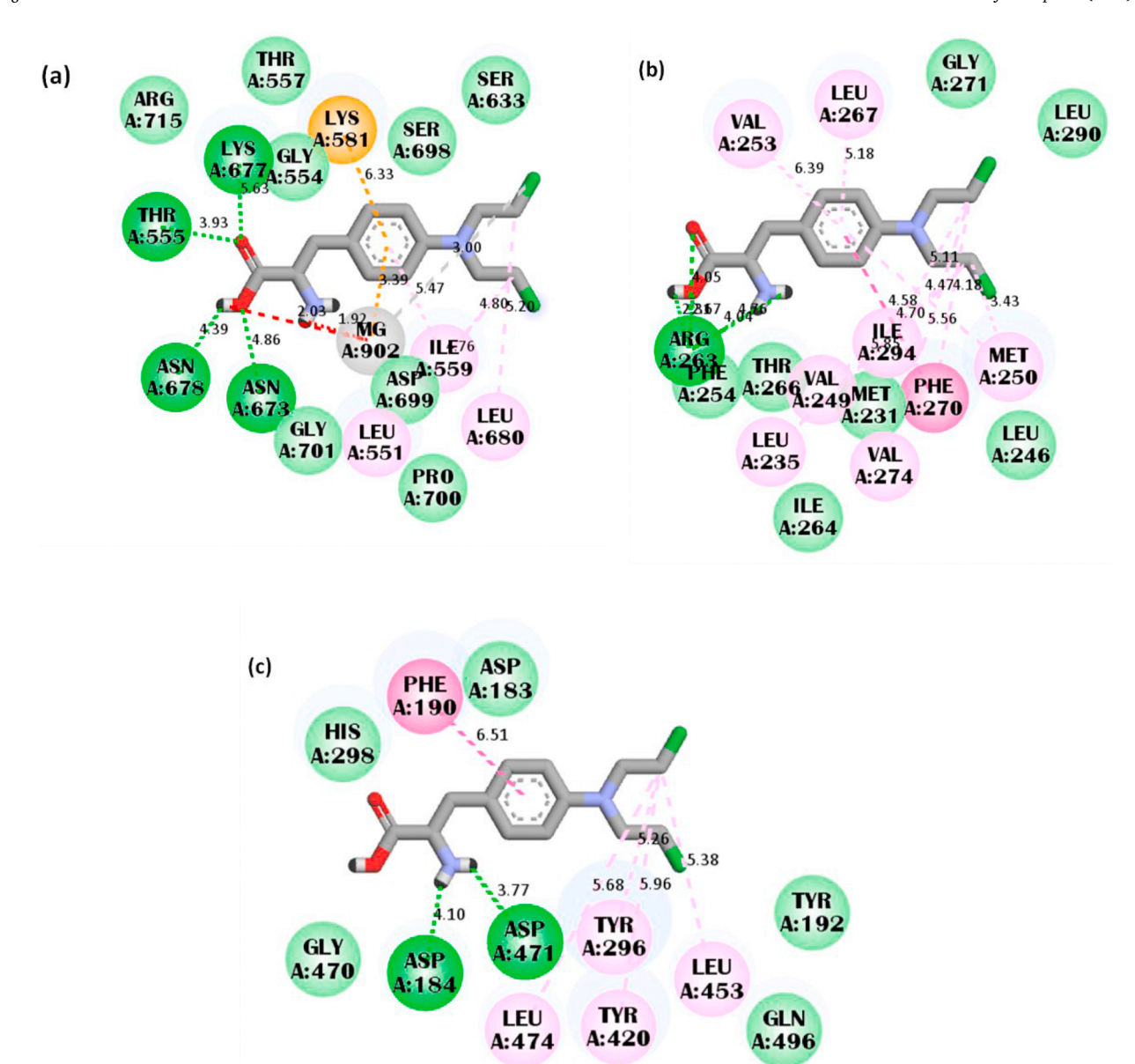


Fig. 11. The Non-covalent weak interactions between 4B2CA-LPA and targeted proteins (a) 4FVR, (b) 3WIX, & (c) 5UUT.

are presented in Table 8 and Fig 11. For this complex, the five conventional carbonyl H-bonds were found between the residues of protein at only ARG263 and the functional groups of NH<sub>2</sub>, OH, & C=O of the ligand with distances 4.76, 4.04, 2.21, 3.67, & 4.05 Å respectively. One  $\pi$ - $\pi$  T-shaped interaction was found at PHE270 and the benzene ring of the 4B2CA-LPA with a distance of 4.58 Å. Three alkyl bonds were identified at ILE85, VAL249, & LEU235 with the CH<sub>2</sub> group of the ligand with distances 5.11, 4.7 & 3.43 Å respectively.

#### 4. Conclusion

In this study, we obtained the global minimum energy structure of anti-blood cancer drug 4-(Bis(2-chloroethyl)amino)-L-phenylalanine and functionalized density functional theory (DFT) calculations. As per these topological results, a novel type of non-covalent interaction of hydrogen-hydrogen attraction forces was found in this molecule by AIM analysis. The strongest delocalization regions are around Cl1-C17-C10 and Cl2-C18-C11 and they are visualized by the ELF map and LOL map respectively. As per the FMOs study, the 4B2CA-LPA was less harmful in these phases because DMSO and water had the highest levels

of softness and minimal hardness, demonstrating the compound's good biological properties. the maximum possibility of a strong nucleophilic attack region is NH<sub>2</sub>, and water has the highest negative energy -36.58 kcal/mol when compared to other solvents, the maximum possibility of a strong electrophilic attack region is CH<sub>2</sub> (C8-H20-H-21), and water has the highest positive energy 52.95 kcal/mol when compared to other solvents. According to the Molecular docking results title compound with the highest binding energy -7.30 kcal/mol was found for *3WIX*: The human myeloid leukaemia cell development protein (hMcl-1) with the compound **4B2CA-LPA**. Molecular docking studies predicted the anticancer activity of the title molecule and future experiments to be tested

# CRediT authorship contribution statement

K. Parveen Begaum: Validation, Visualization, Writing – original draft, Writing – review & editing. T. Prabhu: Conceptualization, Supervision, Data curation, Formal analysis, Funding acquisition, Investigation. M. Thirunavukkarasu: Supervision, Validation, Visualization, Resources. P. Sangeetha: Data curation, Formal analysis, Funding acquisition, Investigation. Saleem Javed: Conceptualization, Data

curation, Formal analysis, Funding acquisition, Software. Jamal M. Khaled: Validation, Visualization, Resources. Ghulam Abbas: Investigation, Methodology, Project administration. S. Muthu: Investigation, Methodology, Project administration.

### **Declaration of Competing Interest**

The authors declare that they have no known competing financial interests or personal relationships that could have appeared to influence the work reported in this paper.

#### Data availability

Data will be made available on request.

#### Acknowledgement

The authors express their sincere appreciation to the Researchers Supporting Project Number (RSPD2023R679), King Saud University, Riyadh, Saudi Arabia.

#### Supplementary materials

Supplementary material associated with this article can be found, in the online version, at doi:10.1016/j.chphi.2023.100272.

#### References

- [1] M.J. Yagi, J.G. Bekesi, M.D. Daniel, J.F. Holland, Increased cancericidal activity of PTT.119, a new synthetic bis-(2-chloroethyl)amino-L-phenylalanine derivative with carrier amino acids, Cancer Chemother. Pharmacol. 12 (1984) 70–76, https://doi.org/10.1007/BF00254592.
- [2] M.J. Yagi, K.J. Scanlon, S.E. Chin, J.G. Bekesi, et al., Mammary tumor and melanoma cell transport of PTT.119, a Bis-(2-Chloroethyl)amino-L-Phenylalanine derivative with carrier amino acids, Chemotherapy 34 (1988) 61–70, https://doi. org/10.1159/000238549.
- [3] A. Riccardi, A. Martinotti, S. Perugini, Cytokinetic changes in two cases of plasma cell leukemia treated with a multipeptide derivative of m-[di(2-chloroethyl) amino]-l-phenylalanine (Peptichemio), Eur. J. Cancer (1965) 14 (1978) 1099–1106, https://doi.org/10.1016/0014-2964(78)90065-8.
- [4] M. Allegrucci, P. Ballerini, L. Romani, Immunopharmacological studies of PTT.119, a new synthetic bis-(2-chloroethyl)amino-L-phenylalanine derivative, Immunopharmacol. Immunotoxicol. 9 (1987) 71–86, https://doi.org/10.3109/ 08923978709035202. PMID: 3450712.
- [5] V.P. Krasnov, E.A. Zhdanova, The synthesis and biological activity of 4-[bis(2-chloroethyl)amino]-DL-, L, and D-phenylalanine amides and peptides, Russ. Chem. Rev. 64 (1995) 1049, https://doi.org/10.1070/RC1995v064n11ABEH000193.
- [6] M.J. Yagi, S.E. Chin, K.J. Scanlon, J.F. Holland, PTT. 119, p-F-Phe-rn-Bis-(2-Chloroethyl)Amino-L-Phe-Met Ethoxy HCI, a new chemotherapeutic agent active against drug-resistant tumor cell lines, Biochem. Pharmacol. 34 (1985) 2347–2354, https://doi.org/10.1016/0006-2952(85)90793-2.
- [7] M.J. Yagi, J.G. Bekesi, Evaluation ofp-F-Phe-m-bis-(2-chloroethyl)amino-L-Phe-Met-ethoxy HCl against transplantable and spontaneous murine neoplasia, Cancer Chemother. Pharmacol. 26 (1990) 215, https://doi.org/10.1007/BF02897202.
- [8] O.S. Aljitawi, S. Abhyankar, S. Ganguly, K. Wolfe, Phase IIa, Open-Label, Randomized, Pharmacokinetic Comparative, Cross-Over Study of Melphalan HCl for Injection (Propylene Glycol-Free) and Alkeran for Injection for Myeloablative Conditioning in Multiple Myeloma Patients Undergoing Autologous Transplantation, Blood 118 (2011) 4512, https://doi.org/10.1182/blood. V118.21.4512.4512.
- [9] R. Potish, L. Adcock, D. Brooker, T.K. Jones Jr, S.H. Levitt, et al., Sequential surgery, radiation therapy, and alkeran in the management of epithelial carcinoma of the ovary, Cancer 45 (1980) 2754–2758, https://doi.org/10.1002/1097-0142 (19800601)45:11<2754::aid-cncr2820451109>3.0.co;2-q.
- [10] B.J. Lee, G. Sahakian, B.D. Clarkson, I.H. Krakoff, Combination chemotherapy of multiple myeloma with Alkeran, Cytoxan, vincristine, prednisone, and BCNU, Cancer 33 (1974) 533–538, https://doi.org/10.1002/1097-0142(197402)33: 2<533::aid-cncr2820330231>3.0.co;2-z.
- [11] S. Haskill, S. Becker, W. Fowler, L. Walton, Mononuclear-cell infiltration in ovarian cancer. I. Inflammatory-cell infiltrates from tumour and ascites material, Br. J. Cancer 45 (1982) 728–736, https://doi.org/10.1038/bjc.1982.114.
- [12] S. Slavin, C. Brodie, The use of bone marrow derived mesenchymal stromal cells for treatment of patients with multiple sclerosis and neurodegenerative disorders – achievements and future goals, Biol. Blood Marrow Transplant. 18 (2012) S257–S258, https://doi.org/10.1016/j.bbmt.2011.12.158.

- [13] A.A. Sidorova, A.V. Grigoriev, E.S. Timofeeva, et al., Determination of dihydroxymelphalan in perfusate, blood plasma, and lung tissue by HPLC-MS: Use in a pharmacokinetic study, J. Anal. Chem. 69 (2014) 377–383, https://doi.org/ 10.1134/S1061934814040108.
- [14] I.D. Davies, J.P. Allanson, R.C. Causon, Rapid determination of the anti-cancer drug Melphalan (AlkeranTM) in human serum and plasma by automated solid phase extraction and liquid chromatography tandem mass spectrometry, Chromatographia 52 (2000) S92–S97, https://doi.org/10.1007/BF02493133.
- [15] T. Bains, A. Lemieux, F. Abar, R.T. Maziarz, Long term engraftment is associated with survival after autologous hematopoietic stem cell transplantation in multiple Myeloma, Biol. Blood Marrow Transplant. 18 (2012) S257, https://doi.org/ 10.1016/j.bbmt.2011.12.154.
- [16] J.I. Brody, M.H. Samitz, Cutaneous signs of cryoparaproteinemia: Control with burst alkeran and prednisone, Am. J. Med. 55 (1973) 211–214, https://doi.org/ 10.1016/0002-9343(73)90170-8.
- [17] S.J. Horning, P.T. Ang, S.A. Rosenberg, R.T. Hoppe, The Stanford experience with combined procarbazine, Alkeran and vinblastine (PAVe) and radiotherapy for locally extensive and advanced stage Hodgkin's disease, Ann. Oncol. 3 (1992) 747-754
- [18] H.R.K. Barber, Role of Radiation Therapy in Management of Ovarian Cancer, Ovarian Carcinoma, Springer, New York, NY, 1993, https://doi.org/10.1007/978-1-9232-3 23.
- [19] A. Boltenberg, S. Furgyik, Placental Proteins (Pp 5, Pp 12 and Pp 14) in ovarian tumors: A preliminary report, Acta Obstet. Gynecol. Scand. 66 (1987) 213–215, https://doi.org/10.3109/00016348709020749.
- [20] M. Strobeck, Multiple myeloma therapies, Nat Rev Drug Discov 6 (2007) 181–182, https://doi.org/10.1038/nrd2269.
- [21] F. Bergel, V.C.E. Burnop, J.A. Stock, Cyto-active amino-acids and peptides. Part II. Resolution of para-substituted phenylalanines and synthesis of p-di-(2-chloroethyl) amino-DL-phenyl[β-14C]alanine, J. Chem. Soc. (1955) 1223–1230, https://doi. org/10.1039/JR9550001223.
- [22] L.F. Larionov, A.S. Khokhlov, E.N. Shkodinskaja, Studies on the anti-tumour activity of p-di-(2-chloroethyl) aminophenylalanine (sarcolysine), Lancet 266 (1955) 169–171, https://doi.org/10.1016/S0140-6736(55)92736-7.
- [23] F. Bergel, J.A. Stock, Cyto-active amino-acid and peptide derivatives. Part I. Substituted phenylalanines, J. Chem. Soc. (1954) 2409–2417, https://doi.org/ 10.1039/JR9540002409.
- [24] B.L. Podlogar, I. Muegge, L.J. Brice, Computational methods to estimate drug development parameters, Curr. Opin. Drug Discov. Dev. 4 (2001) 102–109.
- [25] H. Gökce, F. Sen, Y. Sert, B.F. Abdel-Wahab, B.M. Kariuki, Quantum computational investigation of (E)-1-(4-methoxyphenyl)-5-methyl-N'-(3-phenoxybenzylidene)-1H-1,2,3-triazole-4-carbohydrazide, Molecules 27 (2022) 2193.
- [26] M.J. Frisch, G.W. Trucks, H.B. Schlegel, G.E. Scuseria, M.A. Robb, J.R. Cheeseman, G. Scalmani, V. Barone, B. Mennucci, G.A. Petersson, H. Nakatsuji, M. Caricato, X. Li, H.P. Hratchian, A.F. Izmaylov, J. Bloino, G. Zheng, J.L. Sonnenberg, M. Hada, M. Ehara, K. Toyota, R. Fukuda, J. Hasegawa, M. Ishida, T. Nakajima, Y. Honda, O. Kitao, H. Nakai, T. Vreven, J.A. Montgomery, Jr., J.E. Peralta, F. Ogliaro, M. Bearpark, J.J. Heyd, E. Brothers, K.N. Kudin, V.N. Staroverov, R. Kobayashi, J. Normand, K. Raghavachari, A. Rendell, J.C. Burant, S.S. Iyengar, J. Tomasi, M. Cossi, N. Rega, J.M. Millam, M. Klene, J.E. Knox, J.B. Cross, V. Bakken, C. Adamo, J. Jaramillo, R. Gomperts, R.E. Stratmann, O. Yazyev, A.J. Austin, R. Cammi, C. Pomelli, J.W. Ochterski, R.L. Martin, K. Morokuma, V.G. Zakrzewski, G.A. Voth, P. Salvador, J.J. Dannenberg, S. Dapprich, A.D. Daniels, O. Farkas, J.B. Foresman, J. V. Ortiz, J. Cioslowski, D.J. Fox, Gaussian 09, Revision A.02, Wallingford, CT, (2009) USA.
- [27] M. Thirunavukkarasu, G. Balaji, S. Muthu, et al., Computational spectroscopic investigations on structural validation with IR and Raman experimental evidence, projection of ultraviolet-visible excitations, natural bond orbital interpretations, and molecular docking studies under the biological investigation on N-Benzyloxycarbonyl-L-Aspartic acid 1-Benzyl ester, Chem. Data Collections 31 (2021), 100622, https://doi.org/10.1016/j.cdc.2020.100622.
- [28] M.H. Jamroz, Vibrational energy Distribution Analysis, VEDA 4 Program, Warasaw, Poland, 2004.
- [29] T. Lu, F. Chen, Multiwfn: a multifunctional wavefunction analyzer, J. Comput. Chem. 33 (2012) 580–592.
- [30] The PyMOL Molecular Graphics System, Version 1 5.0.4, Schrodinger LLC, New York, 2009.
- [31] G.M. Morris, D.S. Goodsell, R.S. Halliday, R. Huey, W.E. Hart, R.K. Belew, A. J. Olson, Automated docking using a lamarckian genetic algorithm and empirical binding free energy function, J. Comput. Chem. 19 (1998) 1639–1662.
- [32] M. Thirunavukkarasu, G. Balaji, P. Prabakaran, S. SaleemJaved, S. Muthu, Spectral characterization, solvation effects on topological aspects, and biological attributes of Fmoc-L-glutamic acid 5-tert-butyl ester: An effective reagent in anticancer evaluations. J. Mol. Struct. 1269 (2022). 133793.
- [33] P. Seethalakshmi, C. Palanivel, 4-[Bis(2-chloroethyl)amino]benzaldehyde, IUCrData 2 (2017), x162043, https://doi.org/10.1107/S2414314616020435.
- [34] L. Liu, Y. Shao, J.P. Shi, H.W. Hu, G.Y. Lu, 2-[3-((Z)-2-{4-[Bis(2-chloroethyl) amino]-phenyl}ethenyl)-5,5-dimethylcyclohex-2-en-1- idene]propanedinitrile, Acta Cryst. E67 (2011) o124, https://doi.org/10.1107/S1600536810051068.
- [35] A. Saral, P. Sudha, S. Muthu, A. Irfan, Spectroscopic profiling, DFT computations, molecular docking and molecular dynamic simulation of biologically active 5isoquinolinesulfonic acid, J. Biomol. Struct. Dyn. (2021), https://doi.org/10.1080/ 07391102.2021.2011417.
- [36] M. Thirunavukkarasu, G. Balaj, D. Shanthi, S.Muthu P.Prabakaran, et al., Experimental spectroscopic investigations, solute-solvent interactions, topological analysis and biological evaluations of N-(9-Fluorenylmethoxycarbonyloxy)

- succinimide: An effective agent in anti-breast cancer activity, J. Mol. Liq. 362(2022), 119756.
- [37] S. Muthu, J. Uma Maheswari, T. Sundius, Quantum mechanical, spectroscopic studies (FT-IR, FT-Raman, NMR, UV) and normal coordinates analysis on 3-([2-(diaminomethyleneamino) thiazol-4-yl] methylthio)-N'sulfamoylpropanimidamide, Spectrochimica Acta Part A 108 (2013) 307–318.
- [38] N. Sundaraganesan, S. Ayyappan, et al, FTIR, FT-Raman spectra and ab initio, DFT vibrational analysis of 2,4-dinitrophenylhydrazine, 66 (2007) 17-27.
- [39] DN Sathyanarayana, Vibrational Spectroscopy, 1st ed, new teg Int. Publis, India, 2004.
- [40] R. Kanimozhi, V. Arjunan, An insight into the structure and vibrations of 4-nitroindole and 7-nitroindole by spectroscopic and DFT methods, J. Mol. Struct. 1238 (2021), 130420, https://doi.org/10.1016/j.molstruc.2021.130420, 130420.
- [41] G. Bharathy, J.C. Prasana, S. Muthu, A. Irfan, F.B. Asif, A. Saral, S. Aayisha, Evaluation of electronic and biological interactions between N-[4-(Ethylsulfamoyl) phenyl]acetamide and some polar liquids (IEFPCM solvation model) with Fukui function and molecular docking analysis, J. Mol. Liq. 340 (2021), 117271, https:// doi.org/10.1016/J.MOLLIQ.2021.117271.
- [42] Lei Zhao, Shimei Xiao, Shitian Jiang, Yingxue Jin, Wen Fang, Zhiqiang Wang, Detailed structural investigation of Crizotinib and the exploration of its antitumor potential by DFT calculations and molecular docking, J. Mol. Struct. 1248 (2022), 131530, https://doi.org/10.1016/j.molstruc.2021.131530.
- [43] JAbkowicz-Bieńko Agnieszk, Zdzisław Latajka, Dariusz CBieńko, Danuta Michalska, Theoretical infrared spectrum and revised assignment for paranitrophenol. Density functional theory studies, Chem. Phys. 250 (1999) 123–129, https://doi.org/10.1016/S0301-0104(99)00296-7.
- [44] A. Jeelani, S. Muthu, B. Narayana, Molecular structure determination, Bioactivity score, Spectroscopic and Quantum computational studies on (E)-N'-(4-Chlorobenzylidene)-2-(napthalen-2-yloxy) acetohydrazide, J. Mol. Struct. 1241 (2021), 130558, https://doi.org/10.1016/j.molstruc.2021.130558.
- [45] J.S. Al-Otaibi, Y. Sheena Mary, Y. Shyma Mary, et al., Investigations into the electronic properties of lorlatinib, an anti-cancerous drug using DFT, wavefunction analysis and MD simulations, Viet. J. Chem. 60 (2022) 3.

- [46] S. Muthu, G. Ramachandran, Spectroscopic studies (FTIR, FT-Raman and UV-Visible), normal coordinate analysis, NBO analysis, first order hyper polarizability, HOMO and LUMO analysis of (1R)-N-(Prop-2-yn-1-yl)-2,3-dihydro-1H-inden-1-amine molecule by ab initio HF and density functional methods, Spectrochimica Acta Part A 121 (2014) 394–403.
- [47] J.S. Al-Otaibi, Z. Ullah, Y.S. Mary, Y.S. Mary, DFT investigations on conformational analysis, solvation effects, reactivity studies, chemical descriptors and docking of two anti-cancerous drugs, Lenvatinib and Regorafenib, Viet. J. Chem. 60 (2022) 632–656, https://doi.org/10.1002/vjch.202200013.
- [48] T. Manickavelu, B. Govindrajan, M. Sambantham, et al., Computational investigation, effects of polar and non-polar solvents on optimized structure with topological parameters (ELF, LOL, AIM, and RDG) of three glycine derivative compounds, Struct. Chem. 33 (2022) 1295–1319, https://doi.org/10.1007/ s11224-022-01930-2.
- [49] N. Sheeja, G. Baskar, et al., Covalent interaction, solvent effects, electrochemical, and spectroscopic characterization of novel (4Z)-4-{2-[amino(hydroxy)methyl] hydrazinylidene}-2,6-di(furan-2-yl)-3-methylpiperidin-1-ol derivative- antimicrobial activity study, J. Mol. Liq. 374 (2023), 121272.
- [50] J.S. Al-Otaibi, Zakir Ullah, Y. Sheena Mary, Y. Shyma Mary, Sreejit Soman, et al., Solvation effects, reactivity studies and molecular dynamics of two phosphonic acids – theoretical investigation, Polycycl. Aromat. Compd. (2022), https://doi. org/10.1080/10406638.2022.2126504.
- [51] S. Kim, O.A. Alsaidan, O. Goodwin, Q. Li, E. Sulejmani, Blocking myristoylation of src inhibits its kinase activity and suppresses prostate cancer progression, Cancer Res. 77 (2017) 6950–6962, https://doi.org/10.1158/0008-5472.CAN-17-0981.
- [52] A. Negi, P.V. Murphy, Natural Prod[ucts as Mcl-1 inhibitors: a comparative study of experimental and computational modelling data, Chemistry (Easton) 4 (2022) 983–1009, https://doi.org/10.3390/chemistry4030067.
- [53] S.N. Constantinescu, E. Leroy, Activating Janus kinase pseudokinase domain mutations in myeloproliferative and other blood cancers, Biochem. Soc. Trans. 41 (2013) 1048–1054, https://doi.org/10.1042/BST20130084.